Petrogenesis and tectonic implications of Neoproterozoic, highly fractionated A-type granites from Mianning, South China

Xiao-Long Huang [a,*], Yi-Gang Xu [a,*], Xian-Hua Li [a,b], Wu-Xian Li [a], Jiang-Bo Lan [a], Hui-Huang Zhang [b], Yong-Sheng Liu [c], Yan-Bin Wang [d], Hong-Yan Li [a], Zheng-Yu Luo [a], Qi-Jun Yang [a]

[a] *Key Laboratory of Isotope Geochronology and Geochemistry, Guangzhou Institute of Geochemistry, Chinese Academy of Sciences, Guangzhou 510640, China*
[b] *State Key Laboratory of Lithospheric Evolution, Institute of Geology and Geophysics, Chinese Academy of Sciences, Beijing 100029, China*
[c] *State Key Laboratory of Geological Processes and Mineral Resources, China University of Geosciences, Wuhan 430074, China*
[d] *Institute of Geology, Chinese Academy of Geological Science, Beijing 100037, China*

ARTICLE INFO

ABSTRACT

The origin of Neoproterozoic intrusions (ca. 860–750 Ma) along the western part of the Yangtze Craton has been the subject of debate in recent years, with two competing models proposed. The plume model argues for an extensional setting and emphasizes the role of a superplume in the Rodinia breakup, whereas the arc model argues for the presence of a subduction zone in the Yangtze Craton. As a contribution to this animated dispute, geochronologic and geochemical analyses have been carried out on the Mianning granite, which is the largest pluton ($\sim$700 km^2) in the northern Kangdian rift of the western Yangtze Craton. It is shown that the Mianning granites were emplaced at ca. 780 Ma and display highly fractionated feature (i.e., SiO$_2$ > 75 wt%; Eu/Eu* = 0.03–0.50; enrichment of K, Rb, Th, U, Zr, Hf, Y and REEs; depletion of Nb, Ta, Ba, Sr, P, Eu and Ti). They are metaluminous to strongly peraluminous (A/CNK = 0.93–1.55) and contain abundant perthite and minor alkali riebeckite and sphene, sharing the petrological and geochemical characters of A$_2$-type granites. Positive $\varepsilon_{Nd}(t)$ (2.97–5.24) and zircon $\varepsilon_{Hf}(t)$ (9.2–12.1) values are consistent with a derivation by partial melting of a relatively young crust formed about 1000–900 Ma. Given the general absence of A-type granites in arc settings, the Mianning A-type granites are suggestive of an anorogenic, crustal extensional environment for the western Yangtze Craton during the Neoproterozoic. The data presented in this study are therefore consistent with an intracontinental rift model, but are not sufficient to identify plume involvement in the Neoproterozoic magmatism.

© 2008 Elsevier B.V. All rights reserved.

1. Introduction

In recent years, much geochronological and geochemical data have become available on Neoproterozoic igneous rocks in the Yangtze Block, China. However, interpretations of these data remain highly controversial (e.g., Wang et al., 2004; Zhou et al., 2006, 2007; Li et al., 2006, 2007; Munteanu and Yao, 2007). Li et al. (1999, 2003a,b) attributed the extensive Neoproterozoic magmatism in South China to the activity of a mantle plume associated with the breakup of Rodinia. In contrast, Zhou et al. (2002) suggested that they formed in two major arcs around the Yangtze Block: the Jiangnan arc to the east and the Hannan-Panxi arc to the west (Zhou et al., 2002, 2006, 2007). The debate between plume and arc models (e.g.,

Zhou et al., 2006, 2007; Li et al., 2006, 2007, and references therein) involves interpretation of geochemical and geochronological data. Given the high relevance of this debate to understanding the Neoproterozoic tectonic evolution of the Yangtze Block and its bearing on Rodinia reconstruction models, particularly careful geochemical evaluations are needed.

A-type granite is a distinctive group of granitoids with the following characteristics (Barbarin, 1999): ages of emplacement apparently unrelated to major orogenic events in the vicinity; common contemporaneity with mafic and syenite plutons; Fe-rich mafic mineralogy produced predominantly under reducing conditions; and whole-rock chemistries marked by high alkali, LILE, and HFSE contents, high Fe/Mg ratios, and OIB-type compositions. It is widely accepted that A-type granite formed in a crustal extensional environment, either in post-orogenic or anorogenic settings (Collins et al., 1982; Whalen et al., 1987; Sylvester, 1989; Rogers and Greenberg, 1990; Eby, 1992; Nedelec et al., 1995; Barbarin, 1999; Bonin, 2007). Therefore A-type granites characterize within-plate

areas and can be considered as a diagnostic feature for tectonic discrimination.

Here, we describe A-type granites from Mianning, northern Kangdian rift system (Fig. 1). This large pluton (~700 km^2) has long been considered to have been emplaced during the Triassic-Permian (the geological maps at 1/200,000 scale) or Cretaceous (Liu et al., 1988; Xu et al., 2007a). However, our new zircon U–Pb dating yields an age of ca. 780 Ma, making it contemporaneous with the widespread Neoproterozoic magmatism in South China. Both the typical alkaline mineral assemblage and the geochemical composition indicate an affinity with A-type granites. These A-type granites are temporally and spatially associated with the Suxiong bimodal volcanic rocks (Li et al., 2002a) and widespread mafic dykes (Li et al., 2003b; Lin et al., 2007) in the western Yangtze Block. On the basis of geochemical and Nd–Hf isotopic data, we propose that the Mianning granites were derived from a young crust formed by subduction-related accretion during the Mesoproterozoic. The occurrence of A-type granites provides further evidence that the Neoproterozoic magmatism in South China was formed in an intracontinental rift, rather than subduction-related environment.

2. General geology

South China consists of two major blocks, the Yangtze block in the northwest, and the Cathaysia block in the southeast (Fig. 1a). The N-S trending Kangdian rift along the western margin of Yangtze Block consists of metamorphic complexes, Mesoproterozoic sedimentary strata in greenschist facies (SBGMR, 1991), Neoproterozoic volcanic successions (Lower Sinian volcanic successions) and Neoproterozoic sedimentary strata (Upper Sinian Platform strata). The metamorphic complexes such as the Kangding and Miyi complexes (Fig. 1b) consist of granitic gneisses in upper greenschist to amphibolite facies, which in the past have been interpreted as the Paleoproterozoic or Archean basement (He et al., 1988; SBGMR, 1991). However, recent geochronology indicates that these rocks most likely formed during the Neoproterozoic or Mesoproterozoic (Zhou et al., 2002; Li et al., 2002b). The Suxiong bimodal volcanic rocks, erupted at 803 ± 12 Ma (Li et al., 2002a), constitute the major part of the Lower Sinian system in the northern part of the Kangdian rift (Liu, 1991; Li et al., 2002a), which unconformably overly Mesoproterozoic metamorphic basement slates (Fig. 1). Lower Sinian volcanic successions are conformably overlain by a thick sequence
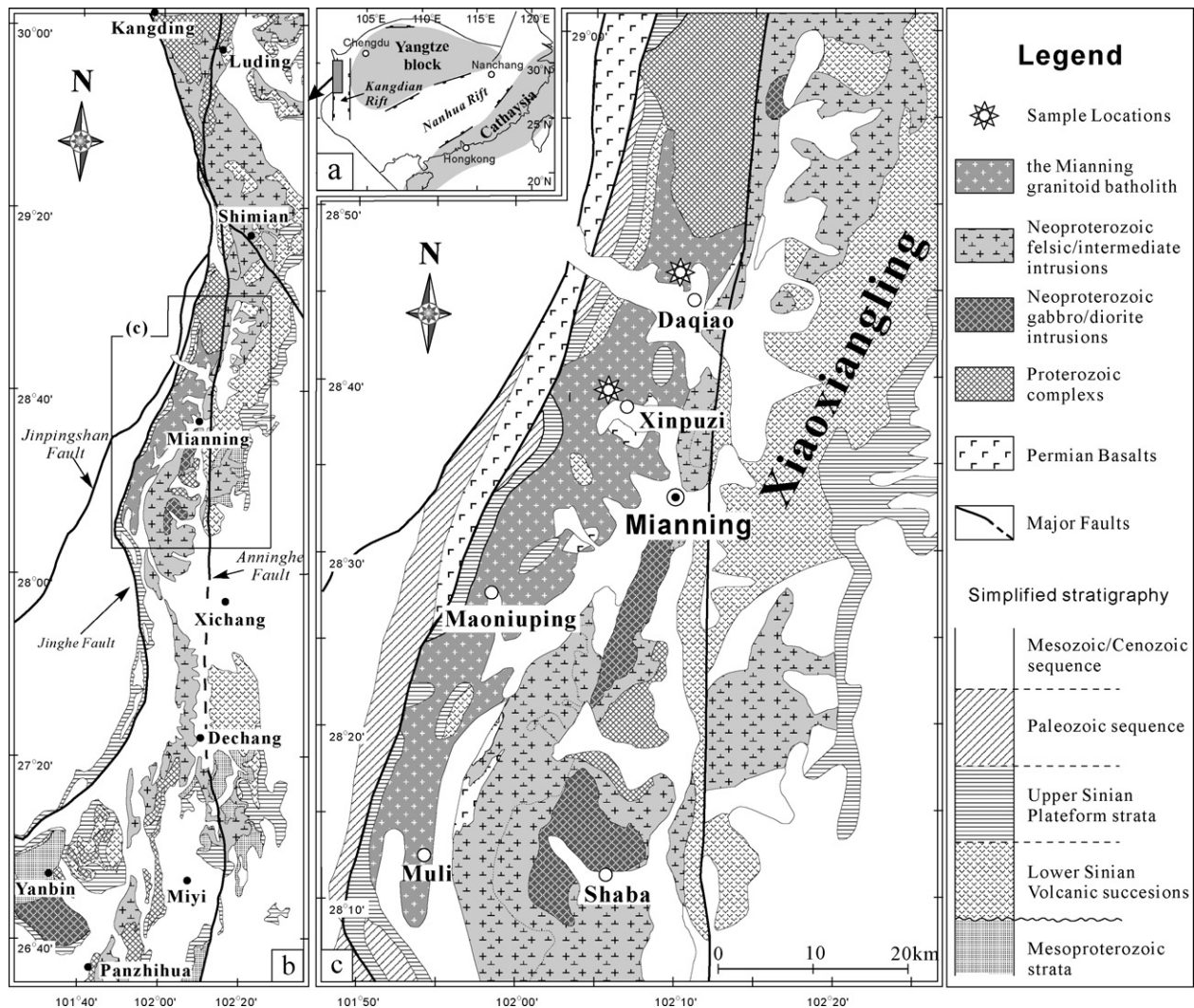
Fig. 1. (a) Neoproterozoic tectonic framework of South China emphasizing two continental rift systems (after Li et al., 1999); (b) simplified geological map of the North Kangdian area, illustrating the distribution of Neoproterozoic intrusions, Proterozoic complexes, Mesoproterozoic strata, the Lower Sinian successions and the Upper Sinian sediments; (c) geological map of the Mianning region, showing the distribution of the Mianning granite batholith and two sample locations (Xinpuzi and Daqiao). Modified after the geological maps in scale of 1/200,000 and Magmatic Rock Map of Sichuan Province (SBGMR, 1991).

of Upper Sinian to Permian strata comprising glacial deposits and clastic, carbonate, and meta-volcanic rocks (Fig. 1) (SBGMR, 1991).

Neoproterozoic felsic to intermediate intrusions are also present mainly along the north–south trending Anninghe fault (Fig. 1b). They intrude the Mesoproterozoic metamorphic rocks, and are overlain by Neoproterozoic successions. The Mianning granite is bounded by the north–south trending Jinghe fault to the west and by the Anninghe fault to the east (Fig. 1c), and covers an area of about 700 km^2. The Mianning granites intrude the Neoproterozoic Suxiong bimodal volcanic successions and the Mesoproterozoic metamorphic rocks to the north, and were unconformably covered by Upper Sinian sediments and some Permian basalts (Fig. 1c). The Mianning granite is composed dominantly of alkali-feldspar granite and minor syenite at the margins.

3. Petrographic characteristics

The samples of this study were collected from two localities in the northern part of the Mianning granite (Daqiao and Xinpuzi; Fig. 1c). They are medium- to fine-grained granite, characterized by equigranular texture or prophyritic texture. The granite is composed dominantly of alkali-feldspar (65–70%), quartz (20–30%) (Fig. 2a), and subordinate hornblende (<3%) and plagioclase (<5%). Magnetite and allanite are the main accessory minerals (<1%), and sphene is occasionally present in some samples (Fig. 2a). Most of the alkali-feldspars in the Mianning granites are perthites with fine and linear exsolutions (Fig. 2b). Some samples show dendritic intergrowths of quartz in alkali-feldspar (Fig. 2c and d). Hornblendes are alkali riebeckite (FeOT = ~34 wt%; Na$_2$O = ~5.5 wt%) and are interstitial to feldspars (Fig. 2c).

4. Analytical methods

Whole-rock major and trace element compositions were obtained by X-ray fluorescence (XRF) and inductively coupled plasma-mass spectrometry (ICP-MS), respectively, at the Guangzhou Institute of Geochemistry, Chinese Academy of Sciences (GIGCAS). Details of procedures are described by Li et al. (2005) and Li (1997), respectively. Precision for REE and other incompatible elements is estimated to be better than 5% from the international USGS reference samples BIR-1 and laboratory standard (ROA-1). In-run analytical precision for Nd is less than 2.5% RSD (relative standard deviation). The Sm/Nd ratios measured by ICP-MS are within 2% uncertainty (Li et al., 2002a), and calculation of ε_{Nd} (t) values for the samples of the present study using these Sm/Nd ratios will result in uncertainties of less than 0.25 ε units, which are negligible for petrogenetic discussion. Neodymium isotopic analyses were carried out using a Micromass Isoprobe multi-collector-inductively coupled plasma mass spectrometry (MC-ICPMS) at GIGCAS, using analytical procedure described by Li et al. (2004). Nd fractions were separated by passing through cation columns followed by HDEHP columns. Measured ^{143}Nd/^{144}Nd ratios were normalized to ^{146}Nd/^{144}Nd = 0.7219. Analyses of standard "Shin Etou" during the period of analyses gave ^{143}Nd/^{144}Nd = 0.512124 ± 11 (2σ).

Zircons were separated using conventional heavy liquid and magnetic techniques and purified by hand-picking under a binocular microscope. They were mounted together with the standard zircons (TEMORA) in epoxy resin. The mount was polished to ensure the exposure of the grains and then was gold-coated. Internal structure of zircons was examined using cathodoluminescence (CL) and back-scattered-electron (BSE) image technique prior to U–Pb isotopic analyses. Zircon U–Pb analyses were performed mainly using a sensitive high-resolution ion microprobe (SHRIMP II) at Beijing SHRIMP Center (the Institute of Geology, Chinese Academy of Geo-

logical Sciences, Beijing); analytical procedures are similar to those described by Williams (1998). The standard TEMORA zircon (age 417 Ma) of RSES was used for correction of interelement fractionation and U, Th and Pb concentrations were determined based on the standard Sri Lankan gem zircon SL13, which has a U concentration of 238 ppm and an age of 572 Ma. Squid (ver. 1.04) and Isoplot (ver. 3.23; Ludwig, 2003) programs were used for raw data reduction and age calculation, and the ^{204}Pb-based method of common Pb correction was applied. Zircon U–Pb analyses of the Xinpuzi granite were performed by laser-ablation-inductively coupled plasma mass spectrometry (LA-ICPMS, Agilent 7500a) at the State Key Laboratory of Geological Processes and Mineral Resources, China University of Geosciences. The laser-ablation system is a GeoLas 2005 (MicroLas, Gottingen, Germany) equipped with a 193 nm ArF-excimer laser and a homogenizing, imaging optical system. A 30 μm spot size and 80 Hz energy density were adopted. Standard 91500 zircon (age 1065 Ma) was used for correction of interelement fractionation, and U, Th and Pb concentrations were determined based on the standard NIST610. The Glitter program (ver. 4.0) was used for raw data reduction and age calculation, and the ^{204}Pb-based method of common Pb correction was applied. Procedures are similar to those described by Yuan et al. (2004). Uncertainties reported in Tables 1 and 2 are all ±1σ. The ages quoted in the text (either ^{207}Pb/^{206}Pb ages or ^{206}Pb/^{238}U ages) are the weighted mean at the 95% confidence level.

In-situ zircon Hf isotopic analyses were carried out on the dated spots using the Neptune MC-ICPMS, equipped with a 193 nm laser, at the Institute of Geology and Geophysics, Chinese Academy of Sciences in Beijing, China. Spot sizes of 40–50 μm with a laser repetition rate of 8 Hz at 100 mJ were used. The detailed analytical technique and data correction procedure are described in Wu et al. (2006). During analyses, the ^{176}Hf/^{177}Hf and ^{176}Lu/^{177}Hf ratios of the standard zircon (91500) were 0.282292 ± 14 (2σ) and 0.00029, similar to the low peaks of ^{176}Hf/^{177}Hf ratios of 0.282284 ± 22 measured using the laser method (Griffin et al., 2006) and the ^{176}Hf/^{177}Hf ratios of 0.282302 ± 8 measured by using solution method (Wiedenbeck et al., 1995).

5. Analytical results

5.1. Zircon U–Pb geochronology

Zircon grains separated for SHRIMP U–Pb and LA-ICPMS U–Pb analyses show well-developed dipyramidal prisms or were fragments of such grains. Most of the zircon grains of sample DQ05-5 are relatively small in size with simple internal oscillatory zonation (Fig. 3a), and those from sample XPZ05-6 have internal oscillatory and sector zonation (Fig. 3b). The analyzed zircons have high concentrations of U (126–1204 ppm) and Th (58–845 ppm) with high Th/U ratios of 0.43–1.01 (Tables 1 and 2). All these are consistent with a magmatic origin.

The zircon SHRIMP U–Pb results for sample DQ05-5 from Daqiao are variable in ^{206}Pb/^{238}U age (525–780 Ma) and have similar ^{207}Pb/^{206}Pb ages within errors (Table 1), suggesting various degrees of radiogenic Pb loss. Four concordant results yield an age of 775 ± 8 Ma and the regression of all the analyses yields an upper intercept age of 780 ± 22 Ma (MSWD = 0.07) (Fig. 3c).

All the analyzed spots in sample XPZ05-6 from Xinpuzi yield ^{206}Pb/^{238}U ages varying between 669 and 771 Ma. Most results are discordant suggesting variable radiogenic Pb loss, and the regression of all the analyses yields an upper intercept age of 773 ± 31 Ma with a small MSWD value (0.18) (Fig. 3d). This age is very similar to the upper intercept age of sample DQ05-5. The upper intercept age obtained by regressing all the data of two samples (DQ05-5

Table 1
SHRIMP U–Pb zircon data of the Mianning granite

Spots	U (ppm)	Th (ppm)	Th/U	^{206}Pb (ppm)	f_{206} (%)	^{207}Pb/^{235}U (1σ)	^{206}Pb/^{238}U (1σ)	^{207}Pb/^{206}Pb (1σ)	^{206}Pb/^{238}U age (Ma)	^{207}Pb/^{206}Pb age (Ma)
XPZ05-6 (Xinpuzi)										
1.1	189	113	0.62	20.8	0.70	1.151 ± 62	0.1271 ± 52	0.0657 ± 23	771 ± 30	796 ± 74
2.1	236	137	0.60	22.2	0.33	0.981 ± 53	0.1093 ± 44	0.0651 ± 23	669 ± 26	777 ± 75
3.1	187	117	0.65	18.9	0.87	1.063 ± 61	0.1168 ± 47	0.0660 ± 26	712 ± 27	807 ± 84
4.1	1204	845	0.73	122	0.14	1.059 ± 43	0.1178 ± 47	0.0652 ± 6	718 ± 27	781 ± 19
5.1	633	396	0.65	66.9	0.04	1.102 ± 45	0.1230 ± 49	0.0650 ± 7	748 ± 28	773 ± 22
6.1	229	130	0.59	21.8	0.66	1.000 ± 51	0.1101 ± 44	0.0658 ± 20	673 ± 26	801 ± 65
7.1r	353	199	0.58	33.4	0.34	1.002 ± 50	0.1098 ± 44	0.0662 ± 20	671 ± 25	814 ± 62
7.2c	593	358	0.62	55.9	0.02	0.990 ± 41	0.1096 ± 44	0.0655 ± 8	671 ± 25	790 ± 24
8.1	203	145	0.74	19.1	0.25	0.998 ± 50	0.1094 ± 44	0.0661 ± 20	669 ± 26	811 ± 62
9.1	326	161	0.51	34.1	0.32	1.102 ± 53	0.1214 ± 49	0.0658 ± 17	739 ± 28	801 ± 55
10.1	934	650	0.72	94.8	0.04	1.078 ± 44	0.1182 ± 46	0.0662 ± 7	720 ± 27	812 ± 23
11.1	640	395	0.64	64.0	0.09	1.045 ± 45	0.1163 ± 47	0.0652 ± 11	709 ± 27	779 ± 37
12.1	376	237	0.65	39.5	0.38	1.106 ± 54	0.1217 ± 51	0.0659 ± 17	740 ± 29	803 ± 55
13.1	522	287	0.57	54.8	0.02	1.091 ± 46	0.1223 ± 49	0.0647 ± 9	744 ± 28	764 ± 29
14.1	303	154	0.53	31.3	0.29	1.091 ± 53	0.1197 ± 48	0.0661 ± 19	729 ± 27	810 ± 60
15.1	235	113	0.50	23.0	0.19	1.029 ± 45	0.1135 ± 45	0.0658 ± 11	693 ± 26	799 ± 37
DQ05-5 (Daqiao)										
1.1	1042	434	0.43	103	0.03	1.025 ± 41	0.1146 ± 45	0.0649 ± 6	700 ± 26	769 ± 18
2.1	381	268	0.73	36.7	0.37	1.005 ± 47	0.1116 ± 45	0.0653 ± 16	682 ± 26	783 ± 51
3.1	314	179	0.59	35.7	0.16	1.189 ± 52	0.1319 ± 53	0.0654 ± 12	799 ± 30	787 ± 37
4.1	212	138	0.68	24.0	0.25	1.188 ± 62	0.1316 ± 53	0.0655 ± 22	797 ± 30	790 ± 69
5.1	416	293	0.73	38.4	0.10	0.967 ± 41	0.1074 ± 43	0.0653 ± 9	658 ± 25	784 ± 30
6.1	385	278	0.75	42.8	0.00	1.166 ± 49	0.1294 ± 52	0.0654 ± 9	785 ± 29	786 ± 29
7.1	215	118	0.57	19.4	0.18	0.943 ± 43	0.1049 ± 42	0.0652 ± 15	643 ± 25	781 ± 49
8.1	277	208	0.78	26.8	0.28	1.016 ± 47	0.1123 ± 45	0.0656 ± 15	686 ± 26	794 ± 48
9.1	367	261	0.73	38.4	0.12	1.093 ± 47	0.1217 ± 49	0.0652 ± 10	740 ± 28	780 ± 34
10.1	250	169	0.70	24.1	0.09	1.013 ± 47	0.1119 ± 45	0.0657 ± 14	684 ± 26	795 ± 46
11.1	323	243	0.78	34.2	0.00	1.108 ± 47	0.1235 ± 49	0.0651 ± 10	751 ± 28	777 ± 31
12.1	720	702	1.01	53.9	0.25	0.786 ± 34	0.0870 ± 35	0.0656 ± 10	538 ± 20	792 ± 33
13.1	792	504	0.66	73.8	0.06	0.972 ± 40	0.1084 ± 43	0.0650 ± 7	664 ± 25	774 ± 24
14.1	285	205	0.74	31.6	0.11	1.165 ± 51	0.1289 ± 52	0.0655 ± 12	781 ± 29	792 ± 37
15.1	338	202	0.62	34.6	0.11	1.069 ± 46	0.1188 ± 48	0.0652 ± 10	724 ± 27	782 ± 35

Table 2
LA-ICPMS U–Pb zircon data of the Mianning granite (XPZ05-6)

Spots	U (ppm)	Th (ppm)	Th/U	^{206}Pb (ppm)	f_{206} (%)	^{207}Pb/^{235}U (1σ)	^{206}Pb/^{238}U (1σ)	^{207}Pb/^{206}Pb (1σ)	^{206}Pb/^{238}U age (Ma)	^{207}Pb/^{206}Pb age (Ma)
01	158	87	0.55	17.5	4.08	0.996 ± 15	0.1131 ± 10	0.0639 ± 11	691 ± 6	737 ± 18
02	388	229	0.59	42.9	0.52	0.994 ± 14	0.1125 ± 10	0.0641 ± 10	687 ± 6	743 ± 15
03	274	141	0.51	28.5	0.85	0.928 ± 14	0.1056 ± 9	0.0638 ± 11	647 ± 5	735 ± 18
04	181	117	0.65	18.9	1.85	0.938 ± 16	0.1065 ± 10	0.0639 ± 12	652 ± 6	737 ± 21
05	392	214	0.55	45.1	0.71	1.029 ± 14	0.1167 ± 10	0.0640 ± 10	712 ± 6	740 ± 15
06	470	278	0.59	51.9	0.39	0.991 ± 14	0.1121 ± 10	0.0641 ± 10	685 ± 6	744 ± 15
07	227	132	0.58	25.8	bdl[a]	1.021 ± 13	0.1154 ± 10	0.0642 ± 9	704 ± 6	748 ± 14
08	239	154	0.64	25.9	0.76	0.966 ± 18	0.1099 ± 10	0.0638 ± 13	672 ± 6	733 ± 23
09	181	107	0.59	21.0	0.84	1.040 ± 15	0.1174 ± 10	0.0643 ± 10	716 ± 6	751 ± 16
10	518	294	0.57	54.7	0.32	0.936 ± 12	0.1073 ± 9	0.0632 ± 9	657 ± 5	716 ± 14
11	542	315	0.58	60.9	0.00	1.005 ± 14	0.1140 ± 10	0.0640 ± 10	696 ± 6	740 ± 15
12	210	101	0.48	26.0	1.35	1.123 ± 17	0.1257 ± 11	0.0648 ± 11	763 ± 6	768 ± 18
13	195	114	0.58	22.6	bdl	1.042 ± 22	0.1177 ± 11	0.0642 ± 14	717 ± 7	749 ± 28
14	286	151	0.53	33.4	bdl	1.052 ± 27	0.1188 ± 12	0.0642 ± 17	724 ± 7	748 ± 36
15	138	73	0.53	16.7	0.86	1.101 ± 21	0.1229 ± 12	0.0650 ± 13	747 ± 7	774 ± 24
16	131	98	0.75	14.9	1.75	1.019 ± 22	0.1152 ± 11	0.0642 ± 14	703 ± 6	747 ± 28
17	338	294	0.87	35.8	bdl	0.949 ± 15	0.1075 ± 10	0.0640 ± 11	658 ± 6	743 ± 18
18	241	125	0.52	28.6	1.22	1.069 ± 17	0.1203 ± 11	0.0644 ± 11	732 ± 6	755 ± 19
19	201	103	0.51	21.6	0.84	0.965 ± 21	0.1092 ± 11	0.0641 ± 15	668 ± 6	746 ± 30
20	423	259	0.61	46.5	0.54	0.981 ± 14	0.1116 ± 10	0.0638 ± 10	682 ± 6	733 ± 16
21	296	169	0.57	34.3	bdl	1.039 ± 18	0.1177 ± 11	0.0640 ± 12	717 ± 6	742 ± 22
22	226	147	0.65	26.7	1.62	1.064 ± 18	0.1199 ± 11	0.0644 ± 12	730 ± 6	754 ± 21
23	126	58	0.46	14.2	bdl	1.007 ± 17	0.1143 ± 10	0.0639 ± 12	697 ± 6	740 ± 20
24	200	130	0.65	21.3	0.62	0.947 ± 20	0.1082 ± 10	0.0635 ± 14	662 ± 6	726 ± 28
25	547	289	0.53	59.9	bdl	0.976 ± 15	0.1112 ± 10	0.0637 ± 11	679 ± 6	731 ± 19
26	403	209	0.52	46.8	0.48	1.050 ± 15	0.1179 ± 10	0.0646 ± 10	718 ± 6	762 ± 15
27	217	186	0.86	25.5	bdl	1.057 ± 24	0.1193 ± 12	0.0643 ± 15	726 ± 7	750 ± 31
28	193	147	0.76	21.5	0.72	1.001 ± 19	0.1132 ± 11	0.0641 ± 14	691 ± 6	746 ± 24
29	161	106	0.66	18.4	bdl	1.023 ± 17	0.1156 ± 10	0.0642 ± 11	705 ± 6	749 ± 19
30	233	118	0.51	26.1	0.69	1.005 ± 16	0.1138 ± 10	0.0641 ± 11	695 ± 6	744 ± 19
31	147	73	0.49	14.7	bdl	0.888 ± 24	0.1014 ± 11	0.0635 ± 18	623 ± 6	725 ± 39
32	428	262	0.61	51.3	0.77	1.082 ± 22	0.1214 ± 12	0.0647 ± 14	739 ± 7	764 ± 26
33	230	115	0.50	28.0	1.75	1.109 ± 19	0.1237 ± 11	0.0650 ± 12	752 ± 6	776 ± 20

[a] bdl denotes for common Pb below the detection limits.
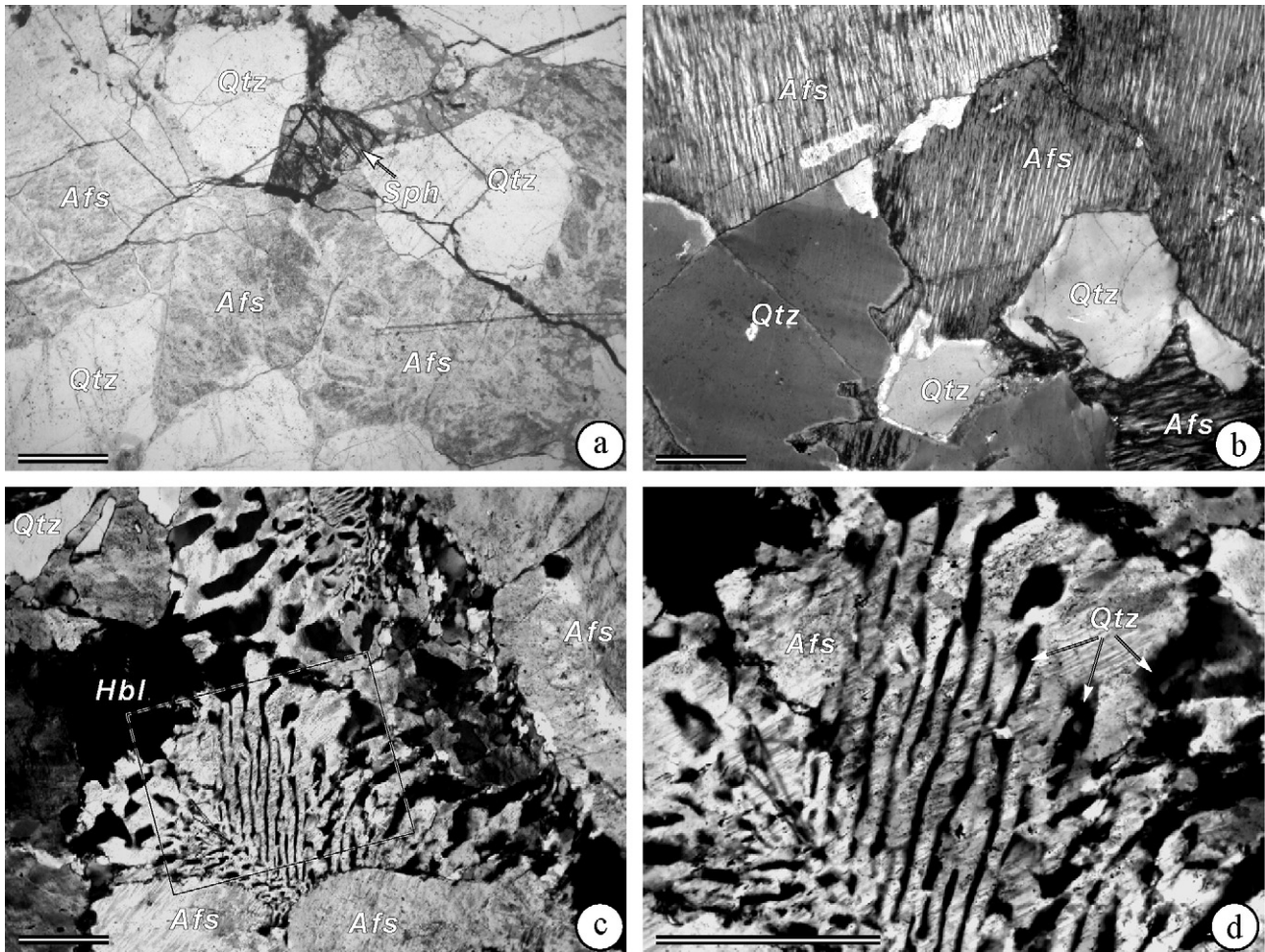
Fig. 2. Petrographic characteristics of the Mianning granites. (a) The granite is dominantly composed of alkali-feldspar (Afs) and quartz (Qtz); sphene (Sph) is locally present interstitial to feldspars and quartz (plane polarized light); (b) alkali-feldspars are perthitic with fine and linear exsolutions (crossed polarized light); (c and d) micrographic texture in the granite, dendritic intergrowths of quartz in perthitic alkali-feldspar (crossed polarized light); the hornblende (Hbl) is angular and interstitial to alkali-feldspars. The length of scale bar is 500 μm.

and XPZ05-6) is 783 ± 18 Ma (Fig. 3e), and the lower intercept age is close to 0 Ma with large error.

We also performed LA-ICPMS U–Pb on 33 zircons of sample XPZ05-6. Like the SHRIMP data, LA-ICPMS results are mostly discordant, but show similar $^{207}\text{Pb}/^{206}\text{Pb}$ ages within errors (Fig. 3f; Table 2). The regression of the data yields an upper intercept age of 767 ± 20 Ma (MSWD = 0.17) and a lower intercept age of 263 ± 130 Ma. The upper intercept age obtained by LA-ICPMS is slightly younger than that of SHRIMP results. Furthermore, the LA-ICP-MS data trend towards a Permian lower intercept age, unlike the lower intercept of the SHRIMP analyses which is close to 0 Ma. Apparently, there is a consistent shift in age between the data from the two analytical systems. The distinct features shown by LA-ICPMS and SHRIMP can be attributed to different volumes sampled by the two dating techniques. Specifically, the LA-ICP-MS analysis ablated a pit of 30–40 μm in depth and of 30 μm in diameter (Fig. 3b) on the same mount of the SHRIMP analyses. The relatively depth penetration may occasionally sample the rim area, which seems to have been subjected to strong thermal perturbation. As a result, the LA-ICP-MS data could have been overprinted by the signal from the rim. Consequently, the resultant lower intercept age of 263 ± 130 Ma likely approximates the time of the thermal event, and the upper intercept age represents a minimum estimate of the true emplacement age. In contrast, the SHRIMP analyses only pen-

etrate a few microns of zircons. High resolution of this technique ensures a core–rim distinction. Furthermore, the upper intercept age of the SHRIMP data is virtually the same as the concordant age of 775 ± 8 Ma constrained by four concordant analyses (Fig. 3c). This suggests that the upper intercept age of SHRIMP data is more reliable than that of the LA-ICP-MS data, although the two upper intercept ages obtained by different technique are similar within errors. We thus suggest that the Mianning alkali-feldspar granites were emplaced at ∼780 Ma.

5.2. Zircon Hf isotopes

Eighteen Lu–Hf isotope analyses were obtained for the zircons of sample XPZ05-6. The initial Hf isotope ratios are calculated at 780 Ma. The zircon $\varepsilon_{\text{Hf}}(t)$ values are positive, ranging from 9.2 to 12.1 with a weighted mean of 10.7 ± 0.4 (Table 3). Corresponding depleted mantle model ages range from 870 to 1004 Ma with a weighted mean of age 933 ± 16 Ma (Table 3).

5.3. Major and trace elements

The samples from Xinpuzi and Daqiao, northern part of the Mianning granite, contain high SiO_2 (75.4–77.9 wt%) and K_2O (4.14–5.53 wt%) contents with high K_2O/Na_2O ratios (1.10–2.05)
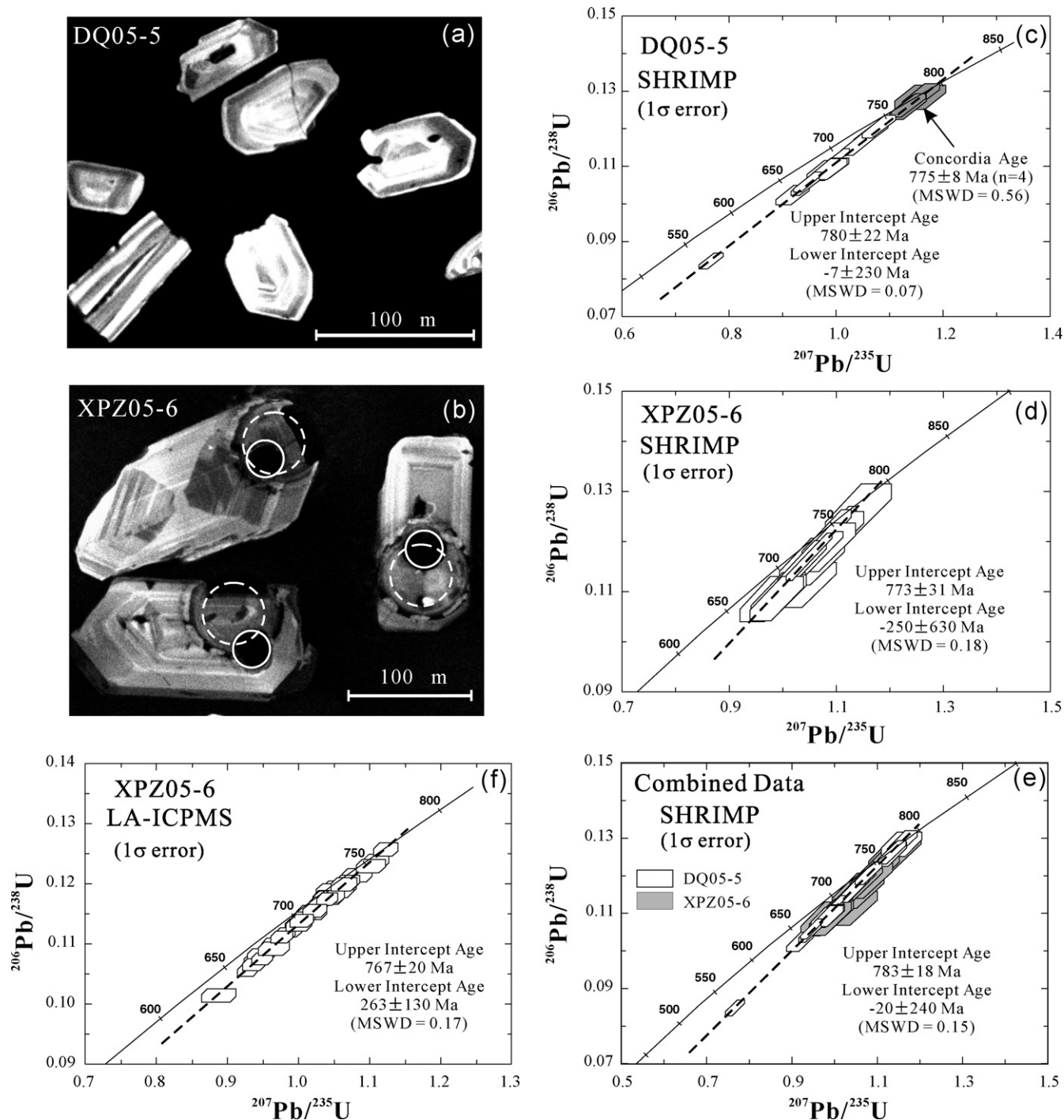
Fig. 3. (a and b) Representative CL images of zircons from DQ05-5 and XPZ05-6, respectively; the circles denote locations of LA-ICP-MS U–Pb dating (30 μm diameter) and in-situ zircon Hf isotopic analyses (40–50 μm diameter); (c–e) concordia diagrams for SHRIMP U–Pb zircon results of two samples (DQ05-5 and XPZ05-6); (f) concordia diagram for LA-ICP-MS U–Pb zircon dating results of XPZ05-6.

(Table 4). They fall in the field of alkaline-granite in the ANOR-Q' diagram (Streckeisen and Le Maitre, 1979) (Fig. 4a). Al_2O_3 content ranges between 11.4 and 13.1 wt%, exhibiting weakly to moderately peraluminous characteristics (A/CNK = 1.00–1.26; Fig. 4b). CaO, MgO and P_2O_5 contents are very low (0.01–0.43, 0.01–0.59 and <0.02 wt%, respectively). For comparison, the data of the samples from Maoniuping, southern Mainning granite (Xu et al., 2007a), are also plotted. It is clear from Figs. 4 and 5 that the Maoniup-

ing samples exhibit a wider range in major element concentrations but lower SiO_2 contents (67–75 wt%) than the northern Mainning granite.

The Mianning granites have high and variable REE contents (Fig. 6a), with slightly fractionated LREE and flat HREE patterns ($(La/Yb)_N$ = 2.5–7.2), and pronounced negative Eu anomalies (Eu/Eu* = 0.18–0.59; Table 4). They have high concentrations of Rb, Th, U, Zr, Hf, Y and HREE (Fig. 6b; Table 4) and strong negative

Table 3
LA-MC-ICPMS zircon Lu–Hf isotope data for the Mianning granite (XPZ05-6)

Spots	$^{176}Yb/^{177}Hf^{a}$	$^{176}Lu/^{177}Hf^{a}$	$^{176}Hf/^{177}Hf^{a}$	$\pm(2\sigma)$	$\varepsilon_{Hf}(t)^{b}$	$\pm(2\sigma)$	T_{DM} (Ma)^{c}	$\pm(2\sigma)$
H-01	0.141126	0.004958	0.282656	0.000031	10.5	1.1	944	48
H-02	0.083061	0.003083	0.282657	0.000025	11.6	0.9	893	37
H-03	0.063108	0.002150	0.282627	0.000019	11.0	0.7	914	28
H-04	0.061335	0.002289	0.282605	0.000022	10.1	0.8	950	32
H-05	0.075118	0.002633	0.282604	0.000018	9.9	0.6	960	27
H-06	0.086582	0.002949	0.282642	0.000017	11.1	0.6	911	26
H-07	0.051666	0.001969	0.282612	0.000019	10.5	0.7	931	28
H-08	0.036764	0.001321	0.282626	0.000033	11.4	1.2	894	47
H-09	0.086956	0.003129	0.282673	0.000035	12.1	1.2	870	52
H-10	0.063190	0.002054	0.282648	0.000022	11.8	0.8	880	32
H-11	0.210331	0.005855	0.282680	0.000026	10.9	0.9	932	42
H-12	0.073583	0.002566	0.282608	0.000019	10.1	0.7	953	28
H-13	0.092140	0.003311	0.282650	0.000021	11.2	0.8	908	32
H-14	0.051419	0.001874	0.282614	0.000020	10.7	0.7	926	29
H-15	0.060527	0.002102	0.282616	0.000019	10.6	0.7	928	28
H-16	0.090257	0.003071	0.282609	0.000018	9.9	0.6	965	27
H-17	0.137419	0.005050	0.282620	0.000025	9.2	0.9	1004	40
H-18	0.109741	0.003723	0.282599	0.000023	9.2	0.8	998	35

[a] The measured values.

[b] Initial Hf isotope ratios are calculated with the reference to the chondritic reservoir at the time of magma crystallization, a decay constant for ^{176}Lu of 1.865×10^{-11} yr^{-1} (Scherer et al., 2001) and the chondritic ratios of $^{176}Hf/^{177}Hf$ (=0.282772) and $^{176}Lu/^{177}Hf$ (=0.0332) (Blichert-Toft and Albarede, 1997) were adopted. $t = 780$ Ma.

[c] Single-stage model ages (T_{DM}) are calculated using the measured $^{176}Lu/^{177}Hf$ ratios, referred to a model depleted mantle with a present-day $^{176}Hf/^{177}Hf$ ratio of 0.28325 and $^{176}Lu/^{177}Hf = 0.0384$ (Griffin et al., 2000).

anomalies of Ba, Sr, Ti and P in the primitive mantle-normalized spidergrams. Despite the relatively high Nb (7.28–44.1 ppm; Table 4) and Ta concentrations (0.82–3.91 ppm; Table 4), negative Nb–Ta anomalies are present with Nb/La ratios ranging between 0.18 and 1.12 (Fig. 6b; Table 4). These characteristics are common with those of the Maoniuping samples (Xu et al., 2007a) and the Suxiong felsic volcanic rocks (Li et al., 2002a) (Fig. 6).

The high SiO$_2$ contents and metaluminous to strong peraluminous (A/CNK = 0.93–1.55; Fig. 4b) characteristics of the Mianning granites are distinct from the metaluminous or weak peraluminous composition (A/CNK < 1.1) of typical I-type granites (Chappell, 1999). The $10,000 \times$ Ga/Al ratios in the Mianning granites are 2.2–4.3, with an average value of 3.5 (Table 4), which is similar to the global average of 3.75 for A-type granites (Whalen et al., 1987). Striking depletions in Ba, Sr, P, Eu and Ti (Fig. 6b) on the spiderdiagram for the Mianning granites are also common features of A-type granite (Collins et al., 1982; Whalen et al., 1987; Wu et al., 2002). Identification of the A-type granites is further supported by the presence of characteristic minerals such as alkali riebeckite,

sphene and perthite (Fig. 2) (Bonin, 2007).

The samples from northern and southern parts of the Mianning granite all straddle the boundary between WPG and Post-COLG in the diagram of Y + Nb vs. Rb, with several samples plotting in the WPG field (Fig. 7). When plotted in Ga/Al vs. Zr or (K$_2$O + Na$_2$O)/CaO vs. Zr + Nb + Ce + Y diagram (Fig. 8a and b), most of the samples fall into the A-type granite field. Their Yb/Nb, Yb/Ta and Ce/Nb ratios are significantly higher than those of OIB, approaching the values of island-arc basalts (IAB) (Fig. 8c and d). According to the geochemical subdivision of A-type granites by Eby (1992), the Mianning granite belongs to A$_2$-type granite.

5.4. Nd isotopes

The Daqiao and Xinpuzi samples of the northern Mianning granite have high initial $^{143}Nd/^{144}Nd$ ratios (0.511784–0.511873) with positive ε_{Nd} (t) values of 2.97–4.71. Similar Nd isotope compositions have been obtained for the Maoniuping samples (ε_{Nd} (t) = 3.22–5.24) (Table 5; Xu et al., 2007a). Single-stage Nd
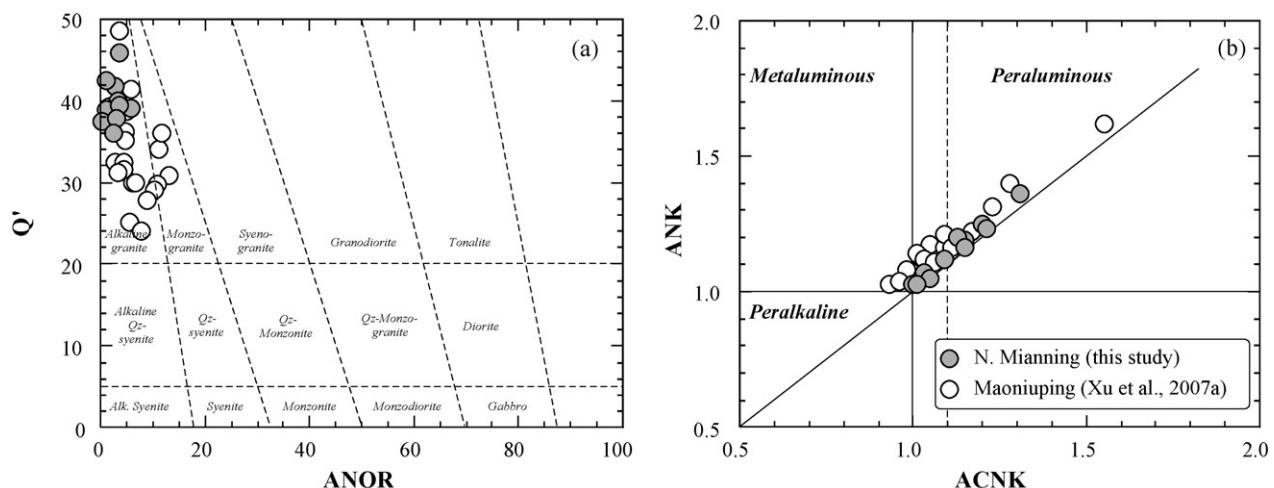
Fig. 4. (a) Q'-ANOR normative composition diagram (Streckeisen and Le Maitre, 1979) for classification of the Mianning granites; Q' = Q/(Q + Or + Ab + An) × 100; ANOR = An/(Or + An) × 100; (b) ANK vs. A/CNK plot showing the metaluminous to peraluminous nature of the Mianning granites; A = Al$_2$O$_3$, N = Na$_2$O, K = K$_2$O, C = CaO (all in molar proportion).

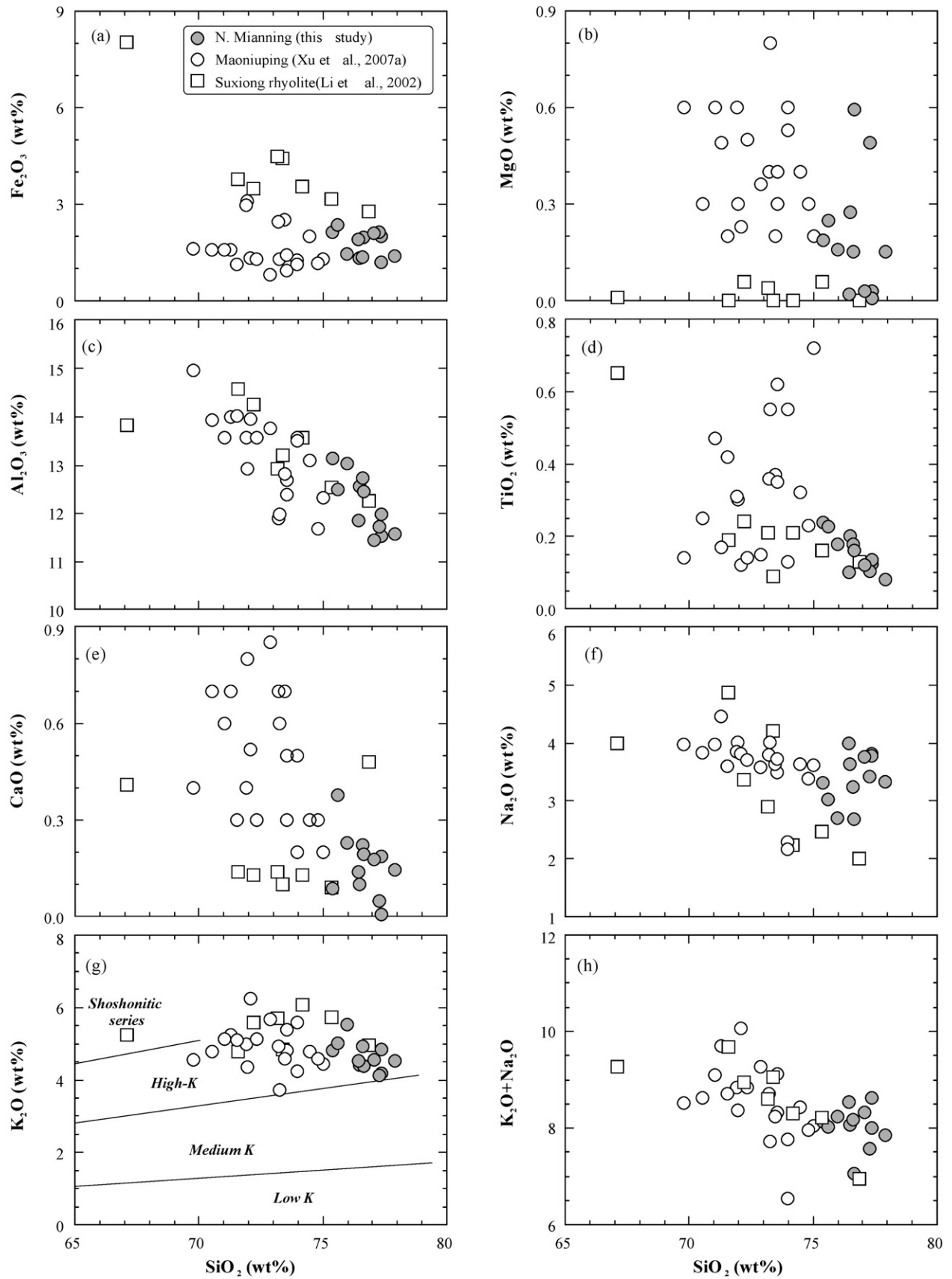**Fig. 5.** Variations of some major elements with SiO_2 of the Mianning granites; the Suxiong rhyolite (Li et al., 2002a) are also shown for comparison.

Table 4
Major (wt%) and trace element (ppm) data of the Mianning granite

| Samples[a]	XPZ05-1	XPZ05-2	XPZ05-3	XPZ05-4	XPZ05-5	XPZ05-6	XPZ05-7	DQ05-5	DQ05-6	DQ05-8	DQ05-9	MDQ-3
SiO_2	75.40	75.62	77.35	77.36	77.29	77.06	76.44	76.46	76.61	76.64	77.92	75.97
TiO_2	0.24	0.23	0.12	0.14	0.10	0.12	0.10	0.20	0.18	0.16	0.08	0.18
Al_2O_3	13.14	12.49	11.54	11.98	11.72	11.44	11.86	12.57	12.73	12.44	11.57	13.02
Fe_2O_3	2.13	2.37	2.00	1.20	2.13	2.09	1.90	1.34	1.37	1.97	1.38	1.47
MnO	0.03	0.03	0.03	0.01	0.02	0.03	0.03	0.02	0.02	0.04	0.02	0.02
MgO	0.19	0.25	0.03	0.01	0.49	0.03	0.02	0.28	0.15	0.59	0.15	0.16
CaO	0.09	0.38	0.19	0.01	0.05	0.18	0.14	0.10	0.22	0.39	0.15	0.43
Na_2O	3.30	3.02	3.81	3.77	3.42	3.76	4.00	3.64	3.24	2.68	3.33	2.70
K_2O	4.83	5.01	4.20	4.84	4.14	4.56	4.53	4.43	4.94	4.38	4.52	5.53
P_2O_5	0.02	0.02	0.00	0.00	0.00	0.00	0.00	0.01	0.01	0.00	0.00	0.01
LOI	0.74	0.47	0.20	0.18	0.31	0.17	0.25	0.42	0.57	0.81	0.34	0.59
Total	100.09	99.88	99.46	99.50	99.67	99.46	99.26	99.47	100.03	100.11	99.46	100.08
A/CNK[b]	1.21	1.13	1.03	1.05	1.15	1.00	1.01	1.15	1.15	1.26	1.09	1.16
K_2O/Na_2O	1.46	1.66	1.10	1.28	1.21	1.21	1.13	1.22	1.52	1.64	1.36	2.05
Al_2O_3/TiO_2	55.6	54.7	93.0	88.6	112.4	93.7	117.7	62.4	71.5	77.9	143.7	73.1
Cr	6.97	15.7	7.82	9.70	8.10	5.87	7.14	9.16	4.56	9.76	10.9	5.90
Ni	1.53	1.53	0.78	3.44	0.36	2.96	2.42	1.28	1.67	3.76	2.00	1.21
Cu	3.74	7.44	5.41	5.66	8.32	5.22	5.14	3.51	12.3	4.33	7.21	4.02
Zn	26.6	21.3	90.1	5.00	97.2	101	98.4	15.6	82.6	33.0	6.80	14.1
Ga	21.2	19.0	25.6	21.5	26.7	23.6	25.6	15.6	15.2	26.8	25.6	19.7
Ge	1.85	1.61	2.45	1.64	2.08	2.18	1.82	1.27	1.52	1.79	1.80	1.80
Cs	0.99	1.02	1.18	0.67	2.43	1.15	10.3	0.85	2.73	2.46	0.51	3.01
Rb	177	170	167	150	222	170	206	131	157	174	169	192
Ba	416	429	33.8	76.9	24.3	32.2	12.7	595	585	694	89.5	309
Sr	30.2	47.4	4.93	6.33	5.24	5.19	2.89	35.4	43.9	46.6	26.5	52.5
Y	60.6	56.0	72.6	59.9	131	73.6	71.7	30.0	24.5	50.6	75.1	48.2
Zr	225	222	357	255	489	283	198	133	126	130	367	135
Hf	9.38	8.60	13.7	10.1	24.1	11.9	8.27	4.96	5.12	5.68	15.8	5.85
Nb	22.3	20.3	26.5	23.9	43.6	25.3	23.6	7.28	7.67	9.40	44.1	15.5
Ta	2.33	2.12	2.18	2.02	3.91	2.22	1.95	0.82	1.00	0.89	3.70	1.87
Pb	12.7	16.8	11.0	6.99	28.2	19.6	21.9	6.53	9.51	9.81	5.99	17.0
Th	23.1	21.3	19.2	16.3	29.9	19.7	14.3	13.2	16.5	12.5	26.1	27.6
U	4.91	4.51	4.47	4.11	7.78	5.03	2.80	2.78	3.16	2.10	5.33	5.95
La	44.8	50.2	47.5	47.2	47.6	42.7	48.6	22.8	30.0	52.9	39.3	46.7
Ce	87.8	105	106	90.1	106	95.9	93.3	49.0	59.6	103	90.9	95.9
Pr	11.7	13.0	14.0	11.0	14.4	12.8	13.5	5.33	6.52	12.2	11.4	11.2
Nd	42.3	45.6	53.1	39.1	55.0	47.0	50.1	18.4	21.4	43.6	42.2	37.5
Sm	8.66	9.04	12.4	7.50	14.3	11.4	11.5	3.72	4.02	8.41	10.6	7.07
Eu	0.76	0.71	0.18	0.19	0.17	0.17	0.15	0.43	0.32	0.72	0.11	0.46
Gd	8.49	8.52	12.3	7.73	16.5	11.8	11.5	3.69	3.72	8.11	11.3	6.37
Tb	1.66	1.59	2.34	1.65	3.61	2.28	2.26	0.75	0.69	1.51	2.32	1.28
Dy	10.2	9.75	13.9	10.7	22.7	13.5	13.3	4.98	4.33	9.13	14.7	8.10
Ho	2.24	2.11	2.80	2.25	4.81	2.83	2.75	1.07	0.94	1.88	3.29	1.74
Er	6.49	6.13	7.96	6.40	13.7	8.02	7.52	3.24	2.74	5.28	9.64	5.18
Tm	1.02	0.93	1.20	0.94	2.07	1.16	1.14	0.50	0.42	0.78	1.52	0.78
Yb	6.78	6.26	7.75	5.86	12.9	7.40	7.44	3.41	2.97	4.97	9.93	5.34
Lu	1.07	0.96	1.22	0.89	1.94	1.11	1.15	0.56	0.48	0.77	1.47	0.84
Eu/Eu*	0.52	0.49	0.21	0.27	0.19	0.21	0.20	0.59	0.50	0.51	0.18	0.45
$10^4 \times$ Ga/Al	3.0	2.9	4.2	3.4	4.3	3.9	4.1	2.3	2.2	4.1	4.2	2.9
Ti/Zr	6.30	6.16	2.08	3.19	1.28	2.59	3.05	9.08	8.50	7.36	1.31	7.92
Zr/Y	3.72	3.97	4.91	4.25	3.72	3.85	2.76	4.42	5.13	2.57	4.89	2.79
Nb/Ta	9.58	9.55	12.14	11.83	11.17	11.38	12.07	8.92	7.70	10.54	11.90	8.30
Nb/La	0.50	0.40	0.56	0.51	0.92	0.59	0.49	0.32	0.26	0.18	1.12	0.33
$(La/Yb)_N$[c]	4.5	5.4	4.1	5.4	2.5	3.9	4.4	4.5	6.8	7.2	2.7	5.9
$(La/Sm)_N$[c]	3.26	3.50	2.42	3.96	2.10	2.37	2.67	3.85	4.69	3.96	2.33	4.16
$(Gd/Yb)_N$[c]	1.02	1.10	1.28	1.07	1.04	1.29	1.26	0.88	1.02	1.32	0.92	0.97
$(Nb/Th)_{PM}$[c]	0.11	0.11	0.16	0.18	0.17	0.15	0.20	0.07	0.06	0.09	0.20	0.07
$(Nb/La)_{PM}$[c]	0.48	0.39	0.54	0.49	0.88	0.57	0.47	0.31	0.25	0.17	1.08	0.32

[a] Sample locations: Xinpuzi (XPZ05-1–7); Daqiao (DQ05-5,6,8,9 and MDQ-3).

[b] A/CNK = $Al_2O_3/(CaO + Na_2O + K_2O)$ (molar ratio).

[c] Subscript N = chondrite-normalized value; PM = primitive mantle-normalized value. Chondrite and PM normalization factors from Taylor and McLennan (1985) and Sun and McDonough (1989), respectively.

model ages of the Mianning granites vary between 1030 and 1480 Ma (Table 5) and are correlated with $f_{Sm/Nd}$ (Fig. 9a). Thus the variable $f_{Sm/Nd}$ values (−0.44 to −0.20; Table 5) suggest that Sm/Nd fractionation during magma differentiation results in relatively unreasonable model ages. Two-stage model ages (T_{DM2} = 960–1090 Ma, Table 5) calculated using the same assumption as Keto and Jacobsen (1987) circumvent this problem, yielding uniform values. As shown in Fig. 9b, ε_{Nd} (t) values of the Mian-

ning granites are similar to those of Yanbian mafic intrusions (800–810 Ma; Zhou et al., 2006), the Suxiong basaltic rocks (803 ± 12 Ma; Li et al., 2002a), the least crustally contaminated Lengqi gabbros (808 ± 12 Ma; Li et al., 2002c) and the crustally contaminated Shimian mafic dykes (760–780 Ma; Lin et al., 2007), but are distinctively lower than those of Yanbian basalts (∼900 Ma; Li et al., 2006) and most primitive Shimian mafic dykes (760–780 Ma; Lin et al., 2007).
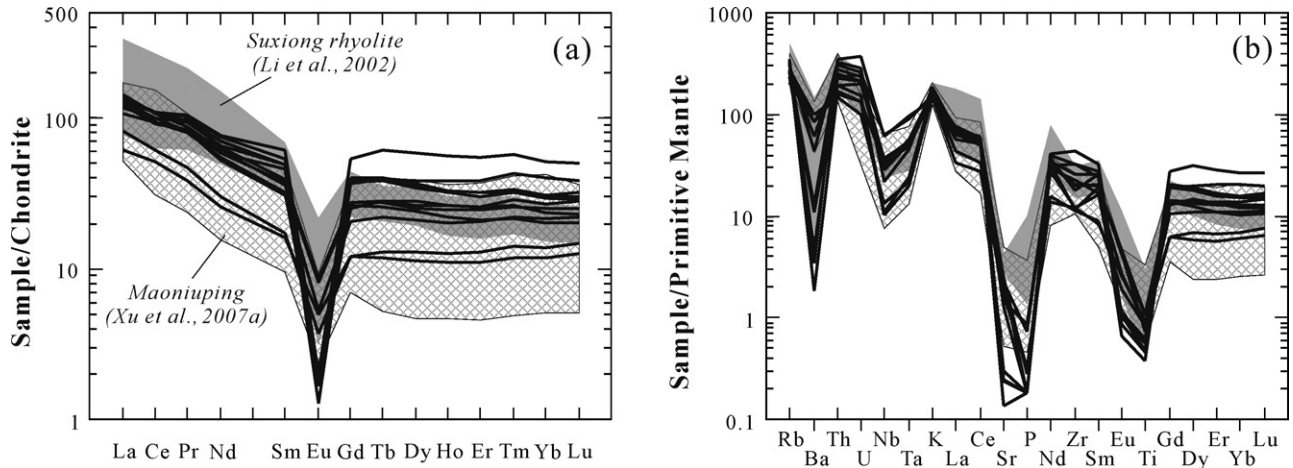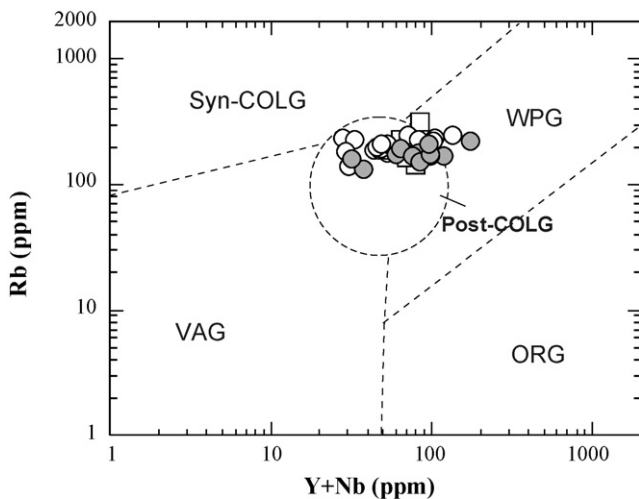
Fig. 6. Chondrite-normalized REE patterns and primitive mantle-normalized trace element spidergrams of the Mianning granites. Chondrite and PM normalization factors from Taylor and McLennan (1985) and Sun and McDonough (1989), respectively.

6. Discussion

6.1. Emplacement ages of the Mianning granite

In the area from Kangding to Panzhihua (i.e., the North Kangdian rift) there were two main episodes of plutonism. The early magmatism is of Neoproterozoic age. Typical examples are the Kangding complexes (764–864 Ma; Zhou et al., 2002), the Suxiong bimodal volcanic successions (803 ± 12 Ma; Li et al., 2002a), the Huangcaoshan granite north of Shimian (786 ± 36 Ma; Shen et al., 2000) and the Shaba gabbro (752 ± 11 Ma; Li et al., 2003b). Although of limited occurrence, currently available data suggest that most Neoproterozoic plutons occur to the north of Xichang (Fig. 1b). Another discrete event of felsic to intermediate intrusions is of Permian ages, including the Panzhihua, Cida and Taihe A-type granites, the Ailanghe I-type granites and the Maomaogou nepheline syenites, occur in the region between Panzhihua and Xichang (the Panxi region; Fig. 1b). These plutons are associated with Emeishan plume activity that resulted in the generation of the continental flood basalts (Luo et al., 2007; Zhong et al., 2007; Shellnutt and Zhou, 2007; Xu et al., 2008).
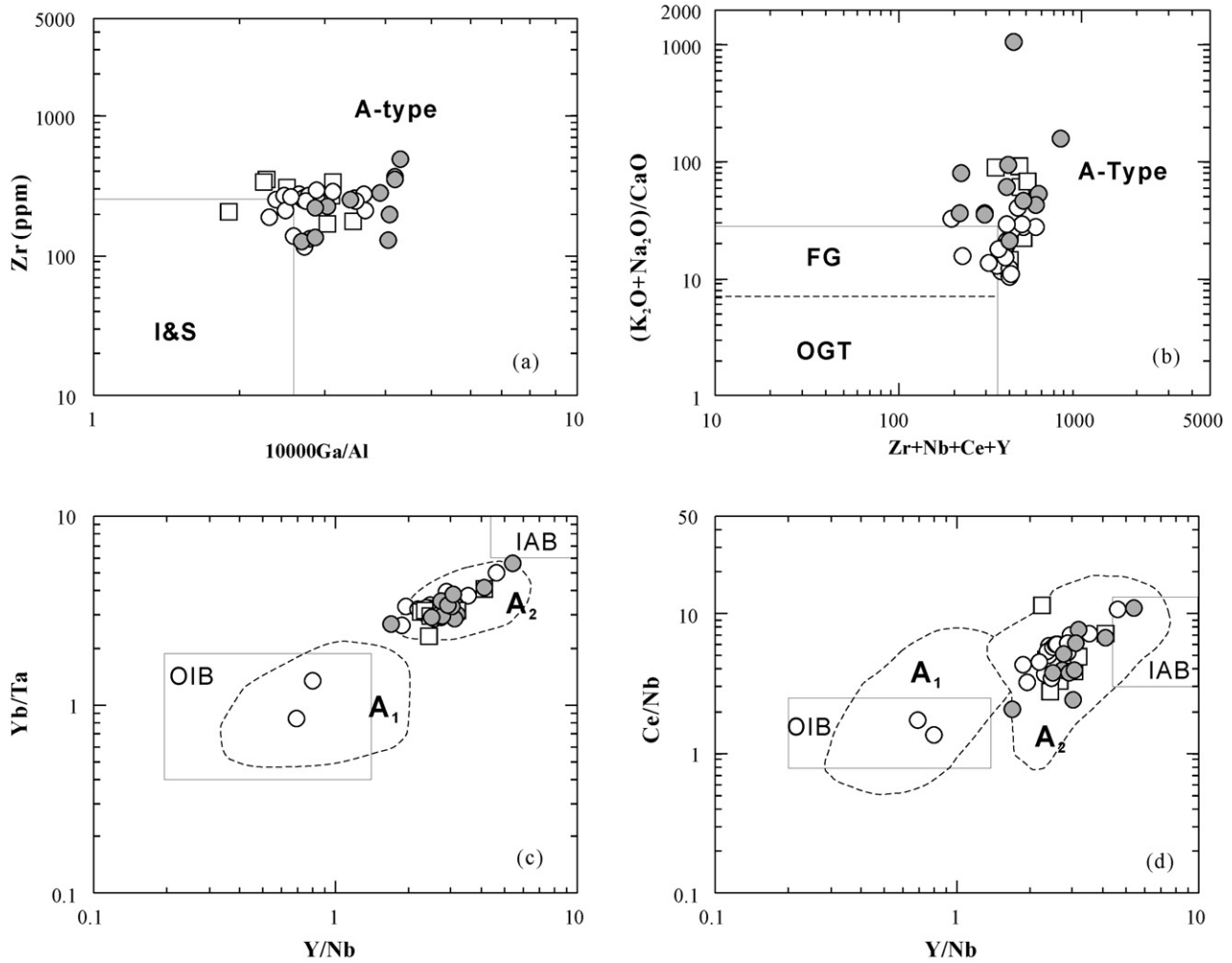
Despite its large exposure, the Mianning granite was one of the least studied plutons in this area and has long been considered to have been emplaced during the Triassic (the geological maps in scale of 1/200,000). Xu et al. (2007a) even suggested a Cretaceous intrusion age based on K–Ar ages of 78–134 Ma (Liu et al., 1988). However, our new zircon U–Pb dating indicates that the Mianning granites were actually emplaced at ~780 Ma (Fig. 3) although they were then severely affected by a thermal perturbation associated with the Permian Emeishan mantle plume (Xu et al., 2004, 2007b). This is also supported by the extensive Pb loss in zircon and the lower intercept age of 263 ± 130 Ma of the discordant ICP-MS data (Fig. 3f). The previously reported K–Ar ages for the Mianning granites probably reflect the Mesozoic thermo-tectonic activity (Boven et al., 2002; Ali et al., 2004).

6.2. Petrogenetic evaluation

6.2.1. Fractional crystallization

The compositional variations (Figs. 5 and 6) of the Mianning granites suggest various degrees of fractional crystallization. Pronounced negative Eu anomalies in the REE patterns require extensive fractionation of feldspar. Plagioclase fractionation would produce negative Sr and Eu anomalies, whereas K-feldspar separation is responsible for the negative Ba anomaly (Wu et al., 2002). The presence of Eu, Sr and Ba negative anomalies in the Mianning granites are hence indicative of fractionation of both plagioclase and K-feldspar. This is further confirmed by the positive correlation between Ba (Sr) and Eu/Eu* (Fig. 10a and b) and negative correlation between K/Rb ratios and Rb (Fig. 10c). In Fig. 10d, Sr decreases from about 100 to 3 ppm, and Ba decreases from about 1000 to 10 ppm. By comparing the composition of the Mianning granites with the vectors of fractionation of different phases, it can be inferred that fractionations of K-feldspar and plagioclase are all important in the evolution of the Mianning granites (Fig. 10d). Moreover, Eu/Eu* values negatively correlate with SiO_2 (Fig. 11a), suggesting that feldspar removal may be responsible for the high silica contents in the Mianning granites.

Ti-bearing minerals such as ilmenite and sphene might be other fractionated phases as suggested by the decrease of TiO_2 with increasing SiO_2 (Fig. 5d). The fractional crystallization of titanium-rich minerals commonly generates negative Nb–Ta and Ti anomalies in basalts (e.g., Xiong et al., 2005). However, this cannot be the main reason for significant negative Nb–Ta anomalies in the Mianning granites because of reverse correlation between Nb/La

Fig. 7. Y + Nb vs. Rb diagram of Pearce (1996) showing that the Mianning granites plot mostly into the post-collision field (Post-COLG) or the within-plate field (WPG). VAG: volcanic arc granites; ORG: ocean ridge granites; WPG: within-plate granites; Syn-COLG and Post-COLG: syn- and post-collision granites. Symbols as in Fig. 5.

Fig. 8. (a and b) Zr vs. 10,000 Ga/Al and $(K_2O + Na_2O)/CaO$ vs. $Zr + Nb + Ce + Y$ classification diagrams of Whalen et al. (1987). The Mianning granites are typical of A-type. FG = fractionated M-, I- and S-type felsic granites; OGT = unfractionated M-, I- and S-type granites. (c and d) Plots of the Mianning A-type granites in Y/Nb vs. Yb/Ta and Ce/Nb diagrams of Eby (1992) for subdivision of A_1- and A_2-type granites. Symbols as in Fig. 5.

Table 5
Nd isotope compositions of the Mianning granite

| Samples	$^{147}Sm/^{144}Nd^a$	$^{143}Nd/^{144}Nd$ (±2σ)	$(^{143}Nd/^{144}Nd)_i$	ε_{Nd} $(t)^b$	$f_{Sm/Nd}^c$	T_{DM1} (Ma)^d	T_{DM2} (Ma)^e
Daqiao and Xinpuzi at north (this study)							
XPZ05-2	0.120	0.512445 ± 8	0.511832	3.90	−0.39	1150	1030
XPZ05-5	0.157	0.512602 ± 10	0.511799	3.26	−0.20	1480	1070
XPZ05-6	0.147	0.512534 ± 10	0.511784	2.97	−0.25	1400	1090
XPZ05-7	0.139	0.512543 ± 9	0.511833	3.93	−0.29	1240	1030
DQ05-5	0.122	0.512498 ± 8	0.511873	4.71	−0.38	1090	990
DQ05-9	0.152	0.512643 ± 8	0.511866	4.58	−0.23	1250	1000
MDQ-3	0.114	0.512438 ± 7	0.511855	4.37	−0.42	1090	1010
Maoniuping at south (Xu et al., 2007a)							
MX-36	0.123	0.512503 ± 15	0.511874	4.74	−0.38	1090	990
MNP-50	0.124	0.512444 ± 12	0.511809	3.47	−0.37	1200	1060
MX-53	0.111	0.512448 ± 16	0.511882	4.89	−0.44	1040	980
MX-56	0.121	0.512417 ± 19	0.511797	3.22	−0.38	1210	1070
MX-58	0.123	0.512458 ± 13	0.511828	3.83	−0.37	1170	1040
MNP-78	0.116	0.512494 ± 11	0.511900	5.24	−0.41	1030	960

^{a} Calculated by using whole-rock Sm and Nd contents.

^{b} ε_{Nd} $(t) = [(^{143}Nd/^{144}Nd)_S/(^{143}Nd/^{144}Nd)_{CHUR} − 1] \times 10{,}000$; $t = 780$ Ma.

^{c} $f_{Sm/Nd} = [(^{147}Sm/^{144}Nd)_S/(^{147}Sm/^{144}Nd)_{CHUR}] − 1$ (Shirey and Hanson, 1986).

^{d} $T_{DM1} = \ln\{[(^{143}Nd/^{144}Nd)_S − (^{143}Nd/^{144}Nd)_{DM}]/[(^{143}Sm/^{144}Nd)_S − (^{147}Sm/^{144}Nd)_{DM}]\}/\lambda$ (DePaolo, 1981).

^{e} $T_{DM2} = T_{DM1} − (T_{DM1} − t)((f_{cc} − f_S)/(f_{cc} − f_{DM}))$ (Keto and Jacobsen, 1987); where S = sample, f_{cc}, f_S and f_{DM} are $f_{Sm/Nd}$ values of the crust, the sample and the depleted mantle, respectively. In the calculation, $(^{143}Nd/^{144}Nd)_{CHUR} = 0.512638$, $(^{147}Sm/^{144}Nd)_{CHUR} = 0.1967$, $(^{143}Nd/^{144}Nd)_{DM} = 0.51315$, $(^{147}Sm/^{144}Nd)_{DM} = 0.2136$, $f_{cc} = −0.6$, $f_{DM} = 0.08592$; $t = 780$ M.
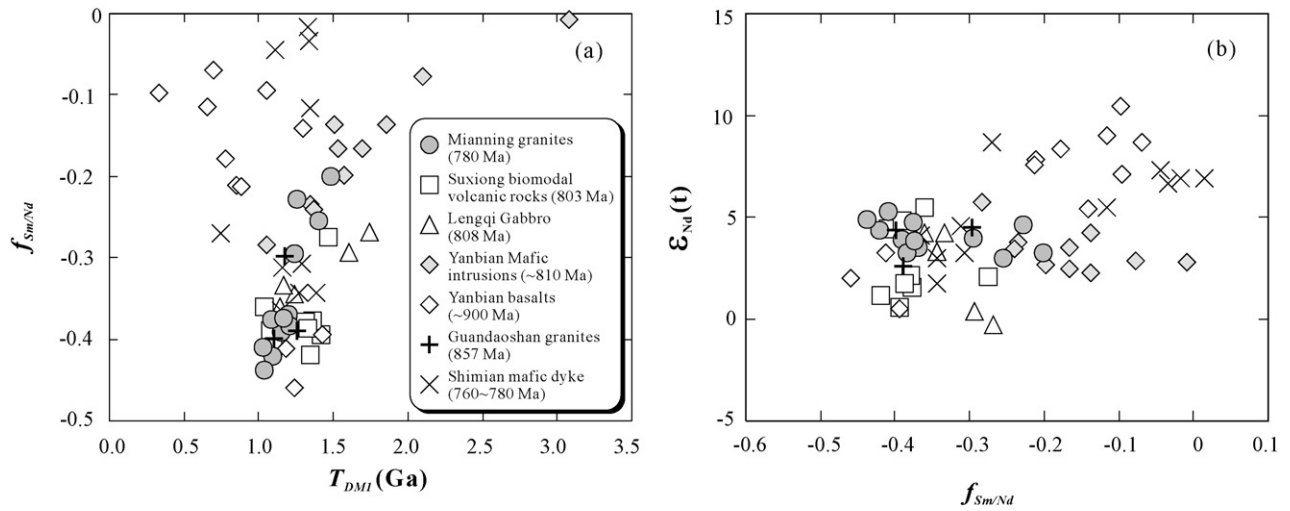
Fig. 9. (a) $f_{Sm/Nd}$ vs. T_{DM1} and (b) ε_{Nd} (t) vs. $f_{Sm/Nd}$ diagrams for the Mianning granites and some Mesoproterozoic to Neoproterozoic mafic intrusions or volcanic rocks at north Kangdian rift. Data sources: Mianning granites (Table 5); Suxiong biomodal volcanic rocks (Li et al., 2002a); Lengqi gabbro (Li et al., 2002c); Yanbian mafic intrusions (Zhou et al., 2006); Yanbian basalts (Li et al., 2006); Shimian mafic dikes (Lin et al., 2007).
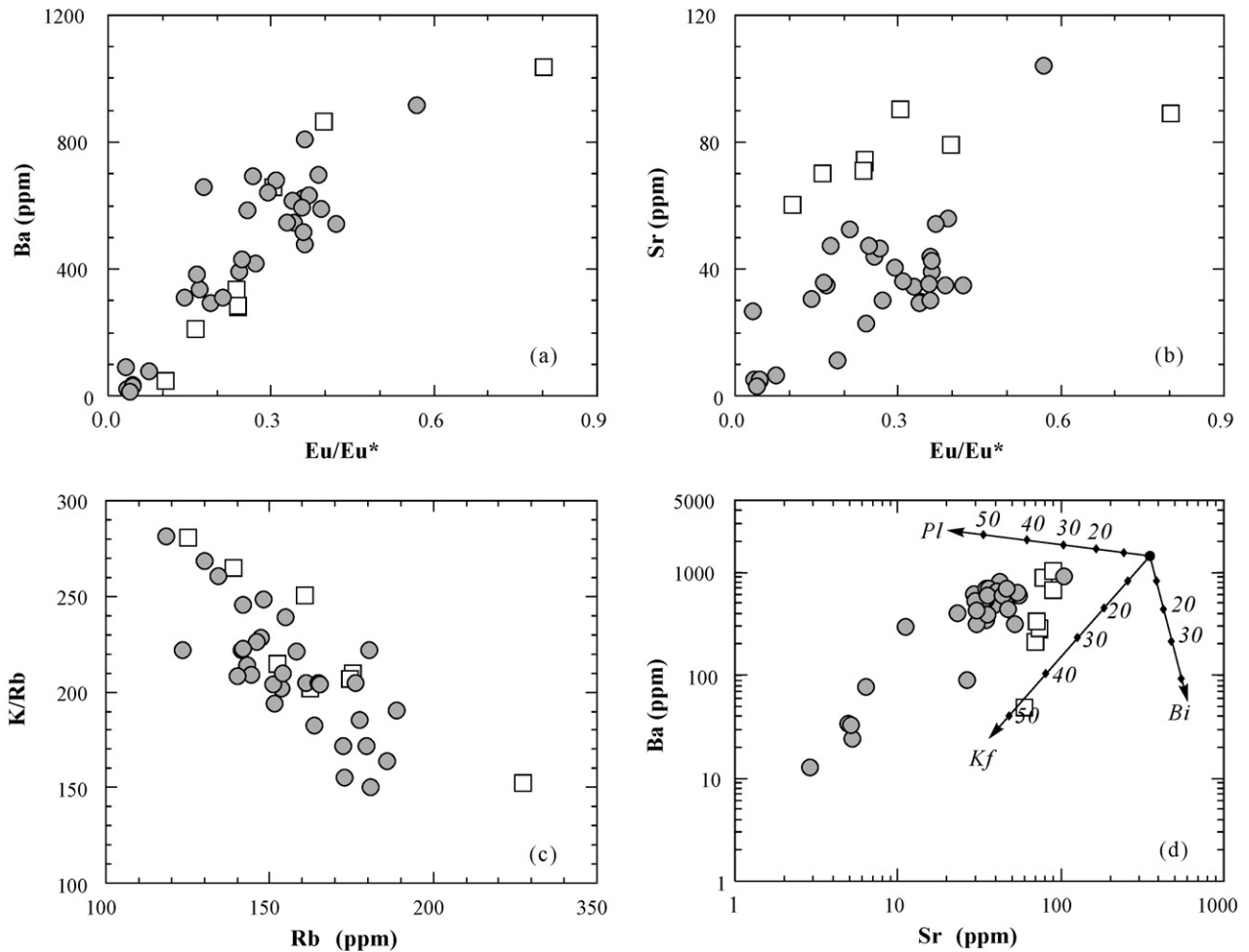
Fig. 10. Diagrams of (a) Ba vs. Eu/Eu*, (b) Sr vs. Eu/Eu*, (c) K/Rb vs. Rb and (d) Ba vs. Sr diagram show that fractionation of K-feldspar played an important role in the differentiation of the Mianning A-type granites; whereas separation of feldspars and biotite appears to have controlled the variation of the Suxiong felsic volcanic rocks. Partition coefficients of Sr and Ba are from Arth (1976). Symbols as in Fig. 9.
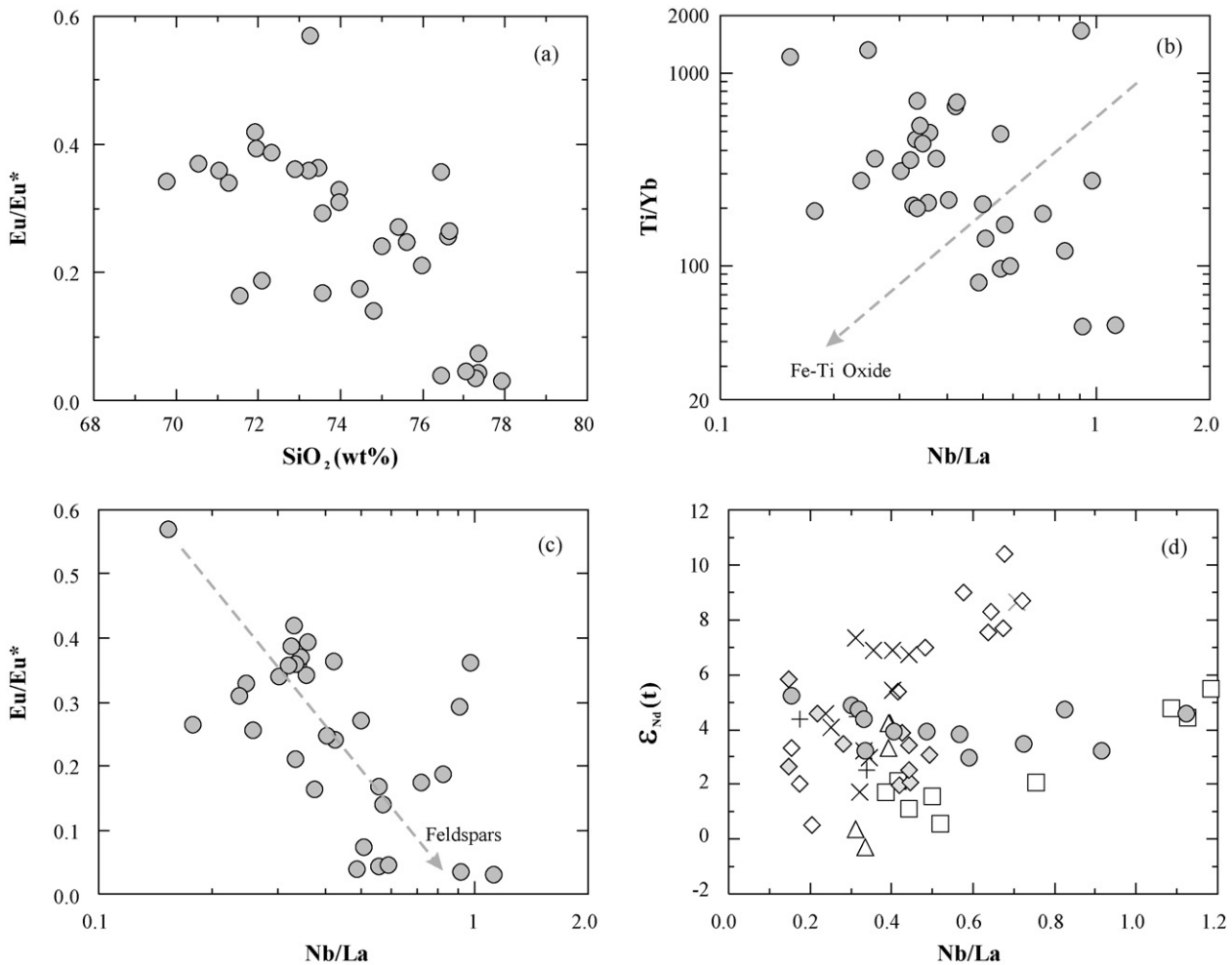
Fig. 11. (a) Eu/Eu* vs. SiO$_2$, (b) Ti/Yb vs. Nb/La, (c) Eu/Eu* vs. Nb/La diagrams for the Mianning granites; (d) ε_{Nd} (t) vs. Nb/La diagram. The latter shows that the initial ε_{Nd} values of the Mianning granites are not correlated to Nb/La, which is distinctively different from the crustal contamination trends of some mafic intrusions or volcanic rocks; t = 780 Ma; data sources and symbols as in Fig. 9.

and Ti/Yb (Fig. 11b). Furthermore, Nb/La increases with decreasing Eu/Eu*, implying that extensive fractionation of feldspars would counterbalance negative Nb–Ta anomalies (Fig. 11c). It is therefore more likely that the negative Nb–Ta anomalies of the Mianning granite inherited those of the sources.

A-type granites may represent differentiation products of mantle-derived magmas with or without crustal contamination through extensive fractional crystallization (Eby, 1990; Turner et al., 1992; Han et al., 1997; Anderson et al., 2003; Zhong et al., 2007). Although crystal fractionation was responsible for the compositional variation of the Mianning granites, they cannot be differentiation products of mantle-derived magmas. The main reasons for this argument include: (1) very small proportion of contemporary mafic rocks in the area (Li et al., 2002a). To produce silicic rocks like the Mianning granites through fractionation of mafic magmas, a significant volume of mafic rocks is required. (2) The lack of correlation between Nb/La and ε_{Nd} (t) (Fig. 11d) or SiO$_2$ precludes an AFC process of mafic magma for the origin of the Mianning granites. Significant crustal contamination can be ruled out given the homogenous Hf isotope composition.

6.2.2. Crustal melting

Partial melting of crustal materials is another important way to generate A-type granites. Examples are low degree melting of granulitic metaigneous sources previously depleted in hydrous felsic melt (Collins et al., 1982; Clemens et al., 1986; Whalen et al., 1987), partial melting of tholeiitic, tonalitic or granodioritic rocks (Creaser et al., 1991; Skjerlie and Johnston, 1993; Patiño Douce, 1997; Frost and Frost, 1997), and partial or complete melting of an alkali-metasomatized crust (Martin, 2006). Eby (1992) identified two sub-groups of A-type granites and suggested that they may have different origins. The A$_1$-type granites represent differentiates of magmas derived from OIB-like sources but emplaced in continental rifts or during intraplate magmatism, whereas the A$_2$-type granites are derived from melting of continental crust or underplated mafic crust that has been through a cycle of continent–continent collision or island-arc magmatism (Eby, 1992). Following this generalization, the Mianning A$_2$-type granites were likely generated by crustal partial melting.

The positive ε_{Nd} (t) (+2.97 to +5.24) and ε_{Hf} (t) (+9.2 to +12.1) preclude highly evolved upper continental crust as the source. Whole-rock Nd model ages range from 960 to 1090 Ma (Table 5). Similar results are obtained by zircon Hf model age (870–1004 Ma; Table 3). These data indicate a relatively young, latest Mesoproterozoic to early Neoproterozoic crustal source for the Mianning granites. As discussed above, the Nb depletion in the Mianning granites did not result from crustal contamination, but was most

likely inherited from the source. We thus speculate that the source of the Mianning granites was an arc-related igneous protolith (Li et al., 2006).

Latest Mesoproterozoic to middle Neoproterozoic (ca. 1050–740 Ma) igneous rocks are widespread along the western margin of the Yangtze Block (Li et al., 2006). Although there is still an hot debate on ages, petrogenesis and tectonic implications of these igneous rocks (Li et al., 2006; Zhou et al., 2006), it is commonly suggested that the orogenic events in western South China took place at 1000–900 Ma (Li et al., 1995). For example, the Kunyang Group along the western margin of the South China Block has depositional age of between ca. 1000 and 960 Ma, representing rocks formed in a synorogenic back-arc basin (Greentree et al., 2006; Li et al., 2006). The zircon Hf model ages of the Mianning granites (870–1004 Ma) are in agreement with the timing (900–1000 Ma) of arc-related magmatism in South China (Li et al., 2006; Ye et al., 2007). The highest ε_{Hf} value calculated for 900 Ma among the analyzed samples is +14.5, very close to the value (+13.8) on the evolution curve of the depleted mantle (Griffin et al., 2000). We thus propose that the Mianning granites were generated by partial melting of a crust formed during the late Mesoproterozoic to early Neoproterozoic. It is conceivable that mafic magmas were derived from asthenospheric mantle or subduction-modified lithospheric mantle in a back-arc setting (Li et al., 2006). Some of them erupted directly, such as the Yanbian basalts (Li et al., 2006), while others may have been underplated. Melting of this crust was induced by heat from mantle-derived hot mafic magmas during crustal extension. Extensive fractionation at shallow crustal levels resulted in the formation of the Mianning granites.

6.3. Tectonic implications

The tectonic regime for the Neoproterozoic magmatism (860–740 Ma) in South China is controversial. One opinion is that this magmatism was generated in an anorogenic setting, probably related to a mantle plume which initiated the breakup of the Rodinia Supercontinent (Li et al., 1999, 2002a, 2003a,b, 2006, 2007). The proponents of this model suggest that the orogenic event terminated by ca. 900 Ma, and that the region was under extension at 860–750 Ma and became part of a failed continental rift (the Kangdian Rift) during the 830–740 Ma interval (Li et al., 2003b, 2006). In this context, the igneous rocks in the region represent melting products associated with the development of the Kangdian Rift (Li et al., 2003b, 2006). The competing model suggests that the orogenic events in western South China lasted until ∼750 Ma, and that mid-Neoproterozoic igneous rocks in the region were formed in a continental arc (the "Hannan-Panxi arc") (Zhou et al., 2002, 2006, 2007).

The data presented in this paper shed some new light on this debate. It is commonly accepted that A-type granites formed in a crustal extensional environment, either in post-orogenic and/or anorogenic settings (Collins et al., 1982; Whalen et al., 1987; Sylvester, 1989; Rogers and Greenberg, 1990; Eby, 1992; Nedelec et al., 1995; Barbarin, 1999; Bonin, 2007). The Mianning A-type granites suggest therefore an intraplate extensional environment for the western margin of the Yangtze Craton at ∼780 Ma. Moreover, the geochemical evaluation and Nd–Hf model ages suggest that the source of the Mianning A-type granites is arc-related material formed about 1000–900 Ma. This interpretation is broadly in agreement with the tectonic evolution model proposed by Li et al. (1999) and Li et al. (2003b), but at odd with the arc model proposed by Zhou et al. (2002). Nevertheless, our data do not provide unequivocal evidence for or against plume involvement in the Neoproterozoic magmatism.

7. Conclusions

On the basis of new geochronological, geochemical and Nd–Hf isotopic data, the following conclusions can be drawn regarding the origin and tectonic setting of the Mianning granites:

(1) Zircon U–Pb dating indicates that the Mianning granites in the north Kangdian rift were emplaced at ∼780 Ma, contemporaneous with the widespread Neoproterozoic anorogenic magmatism in South China.
(2) The Mianning granites are A_2-type granites, generated by partial melting of a crust formed in the latest Mesoproterozoic to early Neoproterozoic (ca. 1000–900 Ma). The magmas were subjected to extensive crystal fractionation at shallow crustal levels, resulting in their highly fractionated nature.
(3) The occurrence of Neoproterozoic A-type granites in south China is indicative of an anorogenic, intracontinental rift regime at ∼780 Ma, rather than an arc setting.

References

Ali, J.R., Lo, C.H., Thompson, G.M., Song, X., 2004. Emeishan basalt Ar–Ar overprint ages define several tectonic events that affected the western Yangtze Platform in the Mesozoic and Cenozoic. J. Asian Earth Sci. 23, 163–178.

Anderson, I.C., Frost, C.D., Frost, B.R., 2003. Petrogenesis of the Red Mountain pluton, Laramie anorthosite complex, Wyoming: implications for the origin of A-type granite. Precamb. Res. 124, 243–267.

Arth, J.G., 1976. Behaviour of trace elements during magmatic processes—a summary of theoretical models and their applications. J. Res. U.S. Geol. Surv. 4, 41–47.

Barbarin, B., 1999. A review of the relationships between granitoid types, their origins and their geodynamic environments. Lithos 46, 605–626.

Blichert-Toft, J., Albarede, F., 1997. The Lu–Hf geochemistry of chondrites and the evolution of the mantle–crust system. Earth Planet. Sci. Lett. 148, 243–258.

Bonin, B., 2007. A-type granites and related rocks: evolution of a concept, problems and prospects. Lithos 97, 1–29.

Boven, A., Pasteels, P., Punzalan, L.E., Liu, J., Luo, X., Zhang, W., Guo, Z., Hertogen, J., 2002. $^{40}Ar/^{39}Ar$ geochronological constraints on the age and evolution of the Permo-Triassic Emeishan Volcanic Province, Southwest China. J. Asian Earth Sci. 20, 157–175.

Chappell, B.W., 1999. Aluminium saturation in I- and S-type granites and the characterization of fractionated haplogranites. Lithos 46, 535–551.

Clemens, J.B., Holloway, J.R., White, A.J.R., 1986. Origin of an A-type granite: experimental constraints. Am. Mineral. 71, 317–324.

Collins, W.J., Beams, S.D., White, A.J.R., Chappell, B.W., 1982. Nature and origin of A-type granites with particular reference to southeastern Australia. Contrib. Mineral. Petrol. 80, 189–200.

Creaser, R.A., Price, R.C., Wormald, R.J., 1991. A-type granites: assessment of a residual-source model. Geology 19, 163–166.

DePaolo, D.J., 1981. A neodymium and strontium isotopic study of the Mesozoic calc-alkaline granitic batholiths of the Sierra Nevada and Peninsular Ranges, California. J. Geophys. Res. 86, 10470–10488.

Eby, G.N., 1992. Chemical subdivision of the A-type granitoids: petrogenetic and tectonic implications. Geology 20, 641–644.

Frost, C.D., Frost, B.R., 1997. Reduced rapakivi-type granites: the tholeiite connection. Geology 25, 647–650.

Greentree, M.R., Li, Z.X., Li, X.H., Wu, H., 2006. Late Mesoproterozoic to earliest Neoproterozoic basin record of the Sibao orogenesis in western South China and relationship to the assembly of Rodinia. Precamb. Res. 151, 79–100.

Griffin, W.L., Pearson, N.J., Belousova, E., Jackson, S.E., O'Reilly, S.Y., van Achterberg, E., Shee, S.R., 2000. The Hf isotope composition of cratonic mantle: LAM-MC-ICPMS analysis of zircon megacrysts in kimberlites. Geochim. Cosmochim. Acta 64, 133–147.

Griffin, W.L., Pearson, N.J., Belousova, E.A., Saeed, A., 2006. Comment: Hf-isotope heterogeneity in zircon 91500. Chem. Geol. 233, 358–363.

Han, B.F., Wang, S.G., Jahn, B.M., Hong, D.W., Kagami, H., Sun, Y.L., 1997. Depleted-mantle source for the Ulungur River A-type granites from North Xinjiang, China: geochemistry and Nd–Sr isotopic evidence, and implications for Phanerozoic crustal growth. Chem. Geol. 138, 135–159.

He, J., Chen, G., Yang, T., Min, J., 1988. The Kandian Grey Gneisses. Chongqing Publishing House, Chongqing (in Chinese).

Keto, L.S., Jacobsen, S.B., 1987. Nd and Sr isotopic variations of Early Paleozoic oceans. Earth Planet. Sci. Lett. 84, 27–41.

Li, X.H., 1997. Geochemistry of the Longsheng Ophiolite from the southern margin of Yangtze Craton, SE China. Geochem. J. 31, 323–337.

Li, Z.X., Zhang, L., Powell, C.M., 1995. South China in Rodinia: part of the missing link between Australia–East Antarctica and Laurentia? Geology 23, 407–410.

Li, Z.X., Li, X.H., Kinny, P.D., Wang, J., 1999. The breakup of Rodinia: did it start with a mantle plume beneath South China? Earth Planet. Sci. Lett. 173, 171–181.

Li, X.H., Li, Z.X., Zhou, H.W., Liu, Y., Kinny, P.D., 2002a. U–Pb zircon geochronology, geochemistry and Nd isotopic study of Neoproterozoic bimodal volcanic rocks in the Kangdian Rift of South China: implications for the initial rifting of Rodinia. Precamb. Res. 113, 135–154.

Li, Z.X., Li, X.H., Zhou, H., Kinny, P.D., 2002b. Grenvillian continental collision in South China: new SHRIMP U–Pb zircon results and implications for the configuration of Rodinia. Geology 30 (2), 163–166.

Li, X.H., Li, Z.X., Zhou, H.W., Liu, Y., Liang, X.R., 2002c. U–Pb ziroch geochronological, geochemical and Nd isotopic study of Neoproterozoic basaltic magmatism in Western Sichuan: petrogenesis and geodynamic implications. Earth Sci. Front. 9 (4), 329–338 (in Chinese with English abstract).

Li, X.H., Li, Z.X., Ge, W., Zhou, H., Li, W., Liu, Y., Wingate, M.T.D., 2003a. Neoproterozoic granitoids in South China: crustal melting above a mantle plume at 825 Ma? Precamb. Res. 122, 45–83.

Li, Z.X., Li, X.H., Kinny, P.D., Wang, J., Zhang, S., Zhou, H., 2003b. Geochronology of Neoproterozoic syn-rift magmatism in the Yangtze Craton, South China and correlations with other continents: evidence for a mantle superplume that broke up Rodinia. Precamb. Res. 122, 85–109.

Li, X.H., Liu, D.Y., Sun, M., Li, W.X., Liang, X.R., Liu, Y., 2004. Precise Sm–Nd and U–Pb isotopic dating of the super-giant Shizhuyuan polymetallic deposit and its host granite, Southeast China. Geol. Mag. 141, 225–231.

Li, X.H., Qi, C.S., Liu, Y., Liang, X.R., Tu, X.L., Xie, L.W., Yang, Y.H., 2005. Petrogenesis of the Neoproterozoic bimodal volcanic rocks along the western margin of the Yangtze Block: new constraints from Hf isotopes and Fe/Mn ratios. Chin. Sci. Bull. 50, 2481–2486.

Li, X.H., Li, Z.X., Sinclair, J.A., Li, W.X., Carter, G., 2006. Revisiting the "Yanbian Terrane": implications for Neoproterozoic tectonic evolution of the western Yangtze Block, South China. Precamb. Res. 151, 14–30.

Li, X.H., Li, Z.X., Sinclair, J.A., Li, W.X., Carter, G., 2007. Reply to the comment by Zhou et al. on: "Revisiting the "Yanbian Terrane": implications for Neoproterozoic tectonic evolution of the western Yangtze Block, South China" [Precambrian Res. 151 (2006) 14-30] [Precambrian Res. 154 (2007) 153-157]. Precamb. Res. 155, 318–323.

Lin, G.C., Li, X.H., Li, W.X., 2007. SHRIMP U–Pb zircon age, geochemistry and Nd–Hf isotopes of the Neoproterozoic mafic dykes from western Sichuan: petrogenesis and tectonic implications. Sci. China Ser. D 50, 1–16.

Liu, H., 1991. Classification of Sinian system. In: Liu, H. (Ed.), The Sinian System in China. Science Press, Beijing, pp. 115–125 (in Chinese).

Liu, Y.R., Jin, M.X., Xing, X.F., Shen, G.F., 1988. Granitoids and Their Metallogenetic Characteristics in Xichang-Middle Part of Yunnan. Chongqing Publishing House, Chongqing (in Chinese).

Ludwig, K.R., 2003. User's Manual for ISOPLOT 3.00: A Geochronological Toolkit for Microsoft Excel, Special Publication no. 4. Berkeley Geochronology Center, p. 71.

Luo, Z.Y., Xu, Y.G., He, B., Shi, Y.R., Huang, X.L., 2007. Geochronologic and petrochemical evidence for the genetic link between the Maomaogou nepheline syenites and the Emeishan large igneous province. Chin. Sci. Bull. 52, 949–958.

Martin, R.F., 2006. A-type granites of crustal origin ultimately result form open-system fenitization-type reactions in an extensional environment. Lithos 91, 125–136.

Munteanu, M., Yao, Y., 2007. The Gaojiacun intrusion: rift- or subduction-related? A discussion on "Revisiting the "Yanbian Terrane": implications for Neoproterozoic tectonic evolution of the western Yangtze Block, South China" by Li et al. (2006). Precamb. Res. 155, 164–167.

Nedelec, A., Stephens, W.E., Fallick, A.E., 1995. The Panafrican stratoid granites of Madagascar: alkaline magmatism in a postcollisional extensional setting. J. Petrol. 36, 1367–1391.

Patiño Douce, A.E.P., 1997. Generation of metaluminous A-type granites by low-pressure melting of calc-alkaline granitoids. Geology 25, 743–746.

Pearce, J.A., 1996. Sources and settings of granitic rocks. Episodes 19, 120–125.

Rogers, J.J.W., Greenberg, J.K., 1990. Late-orogenic, post-orogenic, and anorogenic granites: distinction by major element and trace element chemistry and possible origins. J. Geol. 98, 291–309.

SBGMR (Sichuan Bureau of Geology and Mineral Resources), 1991. Regional Geology of Sichuan Province. Geological Publishing House, Beijing (in Chinese).

Scherer, E., Munker, C., Mezger, K., 2001. Calibration of the Lutetium–Hafnium clock. Science 293, 683–687.

Shellnutt, J.G., Zhou, M.F., 2007. Permian peralkaline, peraluminous and metaluminous A-type granites in the Panxi district, SW China: their relationship to the Emeishan mantle plume. Chem. Geol. 243, 286–316.

Shen, W.Z., Li, H.M., Xu, S.J., Wang, R.C., 2000. U–Pb chronological study of zircons from the Huangcaoshan and Xiasuozi granites in the western margin of Yangtze Plate. Geol. J. Chin. Univ. 6, 412–416 (in Chinese with English abstract).

Shirey, S.B., Hanson, G.N., 1986. Mantle heterogeneity and crustal recycling in Archean granite-greenstone belts: evidence from Nd isotopes and trace elements in the Rainy Lake area, Superior Province, Ontario, Canada. Geochim. Cosmochim. Acta 50, 2631–2651.

Skjerlie, K.P., Johnston, A.D., 1993. Fluid-absent melting behaviour of an F-rich tonalitic gneiss at mid-crustal pressures: implications for the generation of anorogenic granites. J. Petrol. 34, 785–815.

Streckeisen, A., Le Maitre, R.W., 1979. A chemical approximation to the modal QAPF classification of the igneous rocks. Neues Jahrb. Mineral. Abh. 136, 169–206.

Sun, S.-S., McDonough, W.F., 1989. Chemical and isotopic systematics of oceanic basalts: implications for mantle composition and processes. In: Saunders, A.D., Norry, M.J. (Eds.), Magmatism in the Ocean Basins. Geological Society Special Publication no. 42, pp. 313–345.

Sylvester, P.J., 1989. Post-collisional alkaline granites. J. Geol. 97, 261–280.

Taylor, S.R., McLennan, S.M., 1985. The Continental Crust: Its Composition and Evolution. Blackwell, Oxford.

Turner, S.P., Foden, J.D., Morrison, R.S., 1992. Derivation of some A-type magmas by fractionation of basaltic magma: an example from the Padthway Ridge, South Australia. Lithos 28, 151–179.

Wang, X., Zhou, J., Qiu, J., Gao, J., 2004. Comment on "Neoproterozoic granitoids in South China: crustal melting above a mantle plume at ca. 825 Ma?" by Xian-Hua Li et al. (2003). Precamb. Res. 132, 401–403.

Whalen, J.B., Currie, K.L., Chappell, B.W., 1987. A-type granites: geochemical characteristics, discrimination and petrogenesis. Contrib. Mineral. Petrol. 95, 407–419.

Wiedenbeck, M., Alle, P., Corfu, F., Griffin, W.L., Meier, F., Oberli, F., Von Quadt, A., Roddick, J.C., Spiegel, W., 1995. Three natural zircon standards for U–Th–Pb, Lu-Hf, trace element, and REE analyses. Geostand. Newslett. 19, 1–13.

Williams, I.S., 1998. U–Th–Pb geochronology by ion microprobe. In: McKibben, M.A., Shanks III, W.C., Ridley, W.I. (Eds.), Applications of Microanalytical Techniques to Understanding Mineralizing Processes. Rev. Econ. Geol. 7, 1–35.

Wu, F.Y., Sun, D.Y., Li, H., Jahn, B.M., Wilde, S., 2002. A-type granites in northeastern China: age and geochemical constraints on their petrogenesis. Chem. Geol. 187, 143–173.

Wu, F.Y., Yang, Y.H., Xie, L.W., Yang, J.H., Xu, P., 2006. Hf isotopic compositions of the standard zircons and baddeleyites used in U–Pb geochronology. Chem. Geol. 234, 105–126.

Xiong, X.L., Adam, J., Green, T.H., 2005. Rutile stability and rutile/melt HFSE partitioning during partial melting of hydrous basalt: implications for TTG genesis. Chem. Geol. 218, 339–359.

Xu, Y.G., He, B., Chung, S.L., Menzies, M.A., Frey, F.A., 2004. The geologic, geochemical and geophysical conseauences of plume involvement in the Emeishan flood basalt province. Geology 30, 917–920.

Xu, C., Huang, Z., Qi, L., Fu, P., Liu, C., Li, E., Guan, T., 2007a. Geochemistry of Cretaceous granites from Mianning in the Panxi region, Sichuan Province, southwestern China: implications for their generation. J. Asian Earth Sci. 29, 737–750.

Xu, Y.G., He, B., Huang, X.L., Luo, Z.Y., Chung, S.L., Xiao, L., Zhu, D., Shao, H., Fan, W.M., Xu, J.F., Wang, Y.J., 2007b. Identification of mantle plumes in the Emeishan Large Igneous Province. Episode 30, 32–41.

Xu, Y.G., Luo, Z.Y., Huang, X.L., He, B., Xiao, L., Xie, L.W., Shi, Y.R., 2008. Zircon U–Pb and Hf isotope constraints on crustal melting associated with the Emeishan mantle plume. Geochim. Cosmochim. Acta 72, 3084–3104.

Ye, M.F., Li, X.H., Li, W.X., Liu, Y., Li, Z.X., 2007. SHRIMP zircon U–Pb geochronological and whole-rock geochemical evidence for an early Neoproterozoic Sibaoan magmatic arc along the southeastern margin of the Yangtze Block. Gondwana Res. 12, 144–156.

Yuan, H.L., Gao, S., Liu, X.M., Li, H.M., Günther, D., Wu, F.Y., 2004. Precise U–Pb age and trace element determinations of zircon by laser ablation-inductively coupled plasma mass spectrometry. Geostand. Geoanal. Res. 28, 353–370.

Zhong, H., Zhu, W.G., Chu, Z.Y., He, D.F., Song, X.Y., 2007. Shrimp U–Pb zircon geochronology, geochemistry, and Nd–Sr isotopic study of contrasting granites in the Emeishan large igneous province, SW China. Chem. Geol. 236, 112–133.

Zhou, M.F., Yan, D.P., Kennedy, A.K., Li, Y., Ding, J., 2002. SHRIMP U–Pb zircon geochronological and geochemical evidence for Neoproterozoic arc-magmatism along the western margin of the Yangtze Block, South China. Earth Planet. Sci. Lett. 196, 51–67.

Zhou, M.F., Ma, Y., Yan, D.P., Xia, X., Zhao, J.H., Sun, M., 2006. The Yanbian Terrane (southern Sichuan Province, SW China): a Neoproterozoic arc assemblage in the western margin of the Yangtze Block. Precamb. Res. 144, 19–38.

Zhou, M.F., Zhao, J.H., Xia, X.P., Sun, W.H., Yan, D.P., 2007. Comment on "Revisiting the "Yanbian Terrane": implications for Neoproterozoic tectonic evolution of the western Yangtze Block, South China" [Li et al. (2006)]. Precamb. Res. 155, 153–157.